MICROCOPY RESOLUTION TEST CHART

UREAU OF STANDARDS-1963-A

AFWAL-TR-88-3006

A CRITICAL SPEED STUDY FOR AIRCRAFT BIAS PLY TIRES

J.H. Champion

P.M. Wagner

Launch and Recovery Branch

Vehicle Subsystems Division

AD-A193 616

January 1988

Final Report for Period October 1986 - August 1987

DTIC
ELECTE
MAY 1 1 1988
S
E
D

FLIGHT DYNAMICS LABORATORY
AIR FORCE WRIGHT AERONAUTICAL LABORATORIES
AIR FORCE SYSTEMS COMMAND
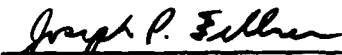WRIGHT-PATTERSON AIR FORCE BASE, OHIO 45433-6553

88 5 09 060

NOTICE

When Government drawings, specifications, or other data are used for any purpose other than in connection with a definitely related Government procurement operation, the United States Government thereby incurs no responsibility nor any obligation whatsoever; and the fact that the government may have formulated, furnished, or in any way supplied the said drawings, specifications, or other data, is not to be regarded by implication or otherwise as in any manner licensing the holder or any other person or corporation, or conveying any rights or permission to manufacture use, or sell any patented invention that may in any way be related thereto.

This report has been reviewed by the Office of Public Affairs (ASD/PA) and is releasable to the National Technical Information Service (NTIS). At NTIS, it will be available to the general public, including foreign nations.

This technical report has been reviewed and is approved for publication.

JOSEPH P. FELLNER
Power Technology Branch
Aerospace Power Division
Aero Propulsion Laboratory

RICHARD A. MARSH, Acting TAM
Batteries and Fuel Cells
Power Technology Branch
Aerospace Power Division

FOR THE COMMANDER

JAMES D. REAMS
Chief, Aerospace Power Division
Aero Propulsion Laboratory

If your address has changed, if you wish to be removed from our mailing list, or if the addressee is no longer employed by your organization please notify AFWAL/POOS-2 W-PAFB, OH 45433 to help us maintain a current mailing list.

Copies of this report should not be returned unless return is required by security considerations, contractual obligations, or notice on a specific document.

REPORT DOCUMENTATION PAGE	Form Approved OMB No. 0704-0188

1a. REPORT SECURITY CLASSIFICATION Unclassified	1b. RESTRICTIVE MARKINGS

2a. SECURITY CLASSIFICATION AUTHORITY	3. DISTRIBUTION/AVAILABILITY OF REPORT
2b. DECLASSIFICATION/DOWNGRADING SCHEDULE	Approved for public release; distribution unlimited

4. PERFORMING ORGANIZATION REPORT NUMBER(S) AFWAL-TR-88-3006	5. MONITORING ORGANIZATION REPORT NUMBER(S)

6a. NAME OF PERFORMING ORGANIZATION Flight Dynamics Laboratory	6b. OFFICE SYMBOL (If applicable) AFWAL/FIEMA	7a. NAME OF MONITORING ORGANIZATION

6c. ADDRESS (City, State, and ZIP Code) Air Force Wright Aeronautical Laboratories Air Force Systems Command Wright-Patterson Air Force Base OH 45433-6553	7b. ADDRESS (City, State, and ZIP Code)

8a. NAME OF FUNDING/SPONSORING ORGANIZATION	8b. OFFICE SYMBOL (If applicable)	9. PROCUREMENT INSTRUMENT IDENTIFICATION NUMBER

8c. ADDRESS (City, State, and ZIP Code)	10. SOURCE OF FUNDING NUMBERS			
	PROGRAM ELEMENT NO. 62201F	PROJECT NO. 2402	TASK NO. 01	WORK UNIT ACCESSION NO. 50

11. TITLE (Include Security Classification) A Critical Speed Study For Aircraft Bias Ply Tires

12. PERSONAL AUTHOR(S) Champion, Jon H; Wagner, Paul M.

13a. TYPE OF REPORT Final	13b. TIME COVERED FROM Oct 86 TO Aug 87	14. DATE OF REPORT (Year, Month, Day) January 1988	15. PAGE COUNT 60

16. SUPPLEMENTARY NOTATION

17. COSATI CODES			18. SUBJECT TERMS (Continue on reverse if necessary and identify by block number)
FIELD	GROUP	SUB-GROUP	Critical Speed, Standing Wave,
01	03		Tire Dynamics, Tire Structural Properties,
11	10		Aircraft Tire, Traction Wave

19. ABSTRACT (Continue on reverse if necessary and identify by block number)

This report describes the derivation and validation of the critical speed equation that predicts the inceptive speed of the standing wave in the tread band of aircraft bias tires.

The critical speed equation is based on the classical theory of a straight beam on an elastic foundation, under tension. Derivations of relations describing each term of the critical speed equation are also presented. These relations describe the effective tire structural properties such as the tread band bending stiffness, the elastic foundation linear spring constant, the belt tension due to inflation pressure, and the tread band effective density.

Dynamometer tests of a 49x17/26PR Type VII Goodyear tire were conducted to validate the critical speed equation. Trends relating critical speed with inflation pressure, tread depth, and loaded vertical deflection were correctly predicted, yielding an average of 2.9-percent error. Keywords:

20. DISTRIBUTION/AVAILABILITY OF ABSTRACT ☑ UNCLASSIFIED/UNLIMITED ☐ SAME AS RPT ☐ DTIC USERS	21. ABSTRACT SECURITY CLASSIFICATION Unclassified
22a. NAME OF RESPONSIBLE INDIVIDUAL Jon H. Champion	22b. TELEPHONE (Include Area Code) (513) 255-2663	22c. OFFICE SYMBOL AFWAL/FIEMA

DD Form 1473, JUN 86   Previous editions are obsolete.   SECURITY CLASSIFICATION OF THIS PAGE

Unclassified

SUMMARY

The governing differential equation describing the vertical motion of the tire tread band as a straight beam on an elastic foundation, under tension, is derived. An assumed mode wave solution is used to derive the critical speed equation from the governing differential equation. The effective tire structural properties used in the critical speed equation are the tread band bending stiffness (EI), the elastic foundation linear spring constant (k), the belt tension due to inflation pressure (T_p), and the tread band effective density (ρ'). These relations are presented as equations 2-21, 2-22, 2-27, and 2-40.

A parametric study is presented, describing the influence of tire inflation pressure, cord half angle, loaded vertical deflection, tread depth, and aspect ratio on critical speed. Those parameters affecting the bending stiffness and tread band tension have the greatest influence on critical speed. These parameters are the cord half angle, tread depth, tire inflation pressure, and aspect ratio. The tire vertical deflection has the least influence on critical speed for a given inflation pressure.

Dynamometer tests of a 49x17/26PR Type VII Goodyear tire were conducted to validate the predicted trends of critical speed versus tire inflation pressure, tread depth, and loaded vertical deflection. Results to date have indicated that the critical speed model has correctly predicted trends. Predicted critical speed values have ranged from -1.5 percent to +13.3 percent error with an average of 2.9 percent error.

Accession For	
NTIS GRA&I	☑
DTIC TAB	☐
Unannounced	☐
Justification	
By	
Distribution/	
Availability Codes	
Dist	Avail and/or Special
A-1	

FOREWORD

This report documents the work during an effort to develop and validate a critical speed prediction model defining the linear speed at which the onset of a standing wave occurs in the tread band of high speed aircraft bias tires. The work was performed by the Launch and Recovery Branch, Vehicle Subsystems Division, Flight Dynamics Laboratory, Air Force Wright Aeronautical Laboratories, Wright-Patterson Air Force Base, Ohio, between October 1986 and August 1987. The project, task, and work unit numbers are 2402, 240201, and 24020150, respectively.

TABLE OF CONTENTS

LIST OF FIGURES

LIST OF TABLES

SECTION I

INTRODUCTION

BACKGROUND

The trend in aircraft and aerospace vehicle design is toward high wing loaded vehicles. This trend is especially evident in the advanced aerospace vehicle concepts currently under study by the Air Force and NASA. Examples of these advanced aerospace vehicle concepts are the National Aerospace Plane and the Objective Vehicle of the Air Force Advanced Launch System Technology Program. Whether having the capability to takeoff, land, or both, in a conventional horizontal fashion, the load and speed requirements of the advanced aerospace vehicle concepts are expected to exceed current state of the art in landing gear performance. One such deficiency involves the upper speed and load limits of current high performance tires. This deficiency is exemplified by the extreme wear problems associated with the Space Shuttle's main landing gear tires during a single landing. The wear is so severe during the first few seconds of touchdown that the tires have been dubbed "half landing tires".

A tire's performance can be measured by its durability, the ability to repeatedly function at design conditions. Aside from wear limits, a tire's long and short term durability may be characterized by its structural integrity. Long term durability may be defined as the tire's ability to retain structural integrity (i.e., carcass/rubber adhesive strength) over a history of stress/temperature cycles typical of its operational use. Short term durability may be defined as the tire's ability to survive at its upper performance limits of speed and load. The critical speed is the tire's upper speed capability characterized by its structural limits such as loss of cohesive and adhesive tread retention due to centrifugal effects or the destructive mechanical deformation of the standing wave. The critical speed can be a measure of the tire's short term durability.

This report presents results of an Air Force study investigating critical speed as a function of the standing wave phenomenon in the tread band region of bias ply aircraft tires.

1

OBJECTIVE

The purpose of this study is to develop a simple closed-form solution that will correctly describe the trends of a bias tire's critical speed as a function of its design and operational characteristics. Critical speed is defined as the velocity at which a standing wave develops in the tread band. The standing wave is represented by a sinusoidal deformation of the tread band around the circumference of the tire. The standing wave is first apparent as the tread elements roll out of the tire footprint. This creates a stress concentration, and in turn, rapid heat generation that may lead to structural failure if critical speed is maintained or exceeded. If the critical speed of bias tires is successfully predicted analytically, then the resulting critical speed model will be used as a tool for the design and assessment of tire designs for application to advanced aerospace vehicles.

APPROACH

A simple closed-form solution described as the critical speed equation was developed as a first-cut prediction tool. Several high-speed tires were selected to conduct critical speed dynamometer tests as a function of tire inflation pressure, tire tread depth, and tire deflection. To date, only a small number of tests have been completed on one tire size, the 49x17/26PR Type VII Goodyear tire. The unvalidated critical speed equation was used to generate an initial test matrix. It was assumed that the critical speed equation was capable of correctly predicting critical speed for a set of test conditions within a band of plus or minus 20 percent. The tires were tested at constant speed, starting at the lower end of the speed band. The test speed was increased from one test cycle to the next until the standing wave was detected visually. Results of the dynamometer tests will be used to make refinements if necessary to both the model and test methodology.

2

THEORY

This section describes the development of the critical speed equation. The governing differential equation from which the critical speed equation is derived describes the oscillatory motion of a straight beam on an elastic foundation, and is considered to be a reasonable representation of the tread band for a bias ply tire subject to the standing wave phenomenon [2][3]. Derivation of the governing differential equation is first described, followed by its solution representing the critical speed associated with the standing wave. Descriptions of the constitutive equations defining the terms of the critical speed equation are also discussed.

DERIVATION OF THE GOVERNING DIFFERENTIAL EQUATION

The variational method is used to derive the governing differential equation. First consider the principle of virtual work which is stated as follows:

"A necessary and sufficient condition for the equilibrium of a system of particles or a continuum system is that the work done by the external forces acting upon the system plus the work done by the internal forces of the system must vanish for any virtual displacement."[1]

Virtual displacements are fictitious motions which are assumed to occur with the actual forces remaining constant. Virtual displacement must be kinematically admissible, (i.e., they can not violate the physical restraints of the system). Virtual work is that work performed during virtual displacements. The principle of virtual work can be expressed as

$$\delta W'_e = -\delta W'_i \qquad (2-1)$$

where,

$\delta W'_e$ = virtual work performed by **external** forces

$\delta W'_i$ = virtual work performed by **internal** forces

If the external and internal forces are considered conservative, then the first-order variation of the potential energy of the internal forces and external forces can be related to virtual work as follows:

$$\delta W'_e = -\delta V \qquad (2-2)$$

$$\delta W'_i = -\delta U \qquad (2-3)$$

3

where,

$$U' = \text{internal potential energy}$$

$$V' = \text{external potential energy.}$$

The principle of the stationary value of the total potential can be derived by combining equations (2-1) through (2-3) and expressed symbolically as

$$\delta(U' + V') = 0 \tag{2-4}$$

where,

$$U' + V' = \text{total potential}$$

The principle of stationary value of the total potential may be stated as:

"A necessary and sufficient condition for the equilibrium of conservative forces acting on a system of particles or a continuum is that the first-order variation of the total potential must vanish for any virtual displacement[1]."

Before taking the first-order variation (δ) and applying the above stated principle, the internal potential energy (U) and external potential energy (V) must be defined for the system of interest. The system under consideration is a straight beam on an elastic foundation under tension, see Figure 1. Only those terms containing the vertical deflection (w) and its derivatives (i.e., $w' = \partial w/\partial x$) are of interest for this study, and only those terms will be retained in the potential energy equations. The vertical displacement of the beam corresponds to the radial (outward) displacement of the tire tread band.
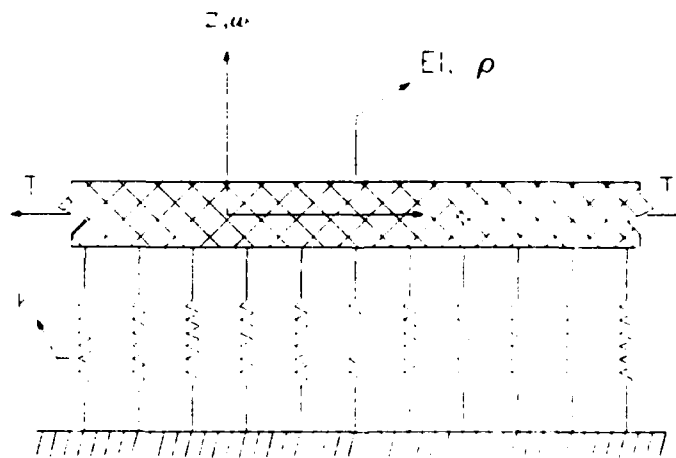
Figure 1. Straight Beam On an Elastic Foundation

The strain energy ($U'_{ке}$) contributes to the internal potential energy (U). Although the behavior of tire materials is nonlinear, when determining the onset of the standing wave it is

4

reasonable to assume linear material properties. Assuming that all stress components other than σ_{xx}, are negligible, and that the material is linear and elastic ($\sigma_{xx} = E\epsilon_{xx}$), the strain energy over an element volume is defined as

$$
\begin{aligned}
U_{se} &= \int_V \left[\int \sigma_{xx} d\epsilon_{xx} \right] dV \\
&= \int_V \left[\int \left(\frac{\sigma_{xx}}{E} \right) d\sigma_{xx} \right) \right] dV \\
&= \frac{1}{2E} \int_V \sigma_{xx}^2 dV.
\end{aligned}
$$

The component of σ_{xx} in terms of w and/or its derivatives for a beam in bending is simply $\sigma_{xx} = -Ezw''$. Substituting this relation for σ_{xx} and assuming a beam of unit width gives

$$
U_{se} = \frac{1}{2} \int_0^L EI(w'')^2 dx \tag{2 - 5}
$$

where,

$$
L = \text{length of the beam.}
$$

The elastic foundation provides an additional term to the internal potential energy. The elastic restraints (i.e., combined effect of tire internal inflation pressure and tire sidewall) are assumed to be evenly distributed over the length of the beam and defined by a linear spring constant k, relating a force per unit area (P) to vertical displacement (w). The internal energy due to the elastic foundation is defined as

$$
\begin{aligned}
U_{ef} &= \int_0^L \int_0^W P dw dx \\
&= \frac{1}{2} \int_0^L kw^2 dx
\end{aligned} \tag{2 - 6}
$$

The net internal energy is the superposition of U_{se} and U_{ef}, and is defined as

$$
\begin{aligned}
U &= U_{se} + U_{ef} \\
&= \frac{1}{2} \int_0^L \left[EI(w'')^2 + kw^2 \right] dx.
\end{aligned} \tag{2 - 7}
$$

The external potential energy has a contribution in terms of w due to the tension force T. This contribution comes about because the point of application of the force T is free to move in the x-direction as bending occurs, and is defined as

$$
V_T = T\Delta(x)
$$

where,

$$
\Delta(x) = \frac{1}{2} \int_0^L (w')^2 dx
$$

5

which is obtained from retaining the first term in the binomial expansion of

$$\Delta(x) = \int_0^L \left[\sqrt{dx^2 + dw^2} - dx \right]$$

Any distribution load $q(x)$ also produces a contribution to the external potential energy V in the form of

$$V_d = -\int_0^L q(x)wdx.$$

The net external energy becomes

$$V = V_T + V_d$$
$$= \int_0^L \left[\frac{T(w')^2}{2} - q(x)w \right] dx. \tag{2-8}$$

The total potential $(U + V)$ is found from equations 2-7 and 2-8, giving

$$U + V = \frac{1}{2} \int_0^L \left[EI(w'')^2 + T(w')^2 + kw^2 - qw \right] dx. \tag{2-9}$$

The principle of stationary value of the total potential can now be applied. As a result of the applied loads, the beam will assume an equilibrium state described by $w(x)$. Taking the first-order variation of the total potential (equations 2-4 and 2-9) gives

$$\int_0^L EIw''\delta w''dx + \int_0^L kw\delta wdx + T\int_0^L w'\delta w'dx - \int_0^L q\delta wdx = 0.$$

Integrating by parts the first and third terms leads to the following expanded form,

$$EI \left[\delta w'(L) - \delta w'(0) \right] w'' - EI \left[\delta w(L) - \delta w(0) \right] w''' + \int_0^L EI(w'')''\delta wdx$$
$$- \int_0^L q\delta wdx + \int_0^L kw\delta wdx + Tw' \left[\delta w(L) - \delta w(0) \right] - T\int_0^L \delta ww''dx = 0.$$

If the structure of interest is a tire tread band which closes upon itself with circumference equal to beam length L, it can be imagined that $x = 0$ corresponds to $x = L$. Therefore, $\delta w(0)$ must equal $\delta w(L)$ and $\delta w'(0)$ must equal $\delta w'(L)$. The first-order variation of the total potential reduces to

$$\int_0^L \left[EI(w'')'' + kw - Tw'' - q \right] \delta wdx = 0 \tag{2-10}$$

Because δw is arbitrary for $0 < x < L$, then the quantity within the brackets of equation 2-10 must always equal zero for the integral to always equal zero. This leads to the following differential equation describing the equilibrium of a straight beam on an elastic foundation,

$$EI(w'')'' - Tw'' + kw - q = 0$$

6

or,

$$EI \left(\frac{\partial^4 w}{\partial x^4} \right) - T \left(\frac{\partial^2 w}{\partial x^2} \right) + kw = q. \qquad (2-11)$$

The oscillatory motion of a straight beam on an elastic foundation can now be obtained by allowing the distributed load $q(x)$ to represent the D'Alembert force $-\rho \frac{\partial^2 w}{\partial t}$, which leads to the equation

$$EI \left(\frac{\partial^4 w}{\partial x^4} \right) - T \left(\frac{\partial^2 w}{\partial x^2} \right) + kw + \rho_m \left(\frac{\partial^2 w}{\partial t^2} \right) = 0. \qquad (2-12)$$

where, t = time and ρ_m = tread mass per unit length.

DERIVATION OF THE CRITICAL SPEED EQUATION

Critical speed is defined as the velocity at which a standing wave develops in the tread band. The critical speed equation is derived by considering an assumed mode as the wave solution to the governing differential equation (equation 2-12), taking the form

$$w = \sin a(x - vt) \qquad (2-13)$$

where, a is a constant and v is the wave speed. Substituting equation 2-13 and its derivatives into equation 2-12 gives

$$EIa^4 + Ta^2 + k - \rho_m a^2 v^2 = 0. \qquad (2-14)$$

Centrifugal effects contribute to the tread tension (T). This implies that T is a function of velocity. It will be demonstrated in the discussion on structural properties that T will have the form

$$T = T_p(\text{pressure effect}) + \alpha v^2(\text{centrifugal effect}) \qquad (2-15)$$

Since the centrifugal effect depends on tread band density, it may be combined with the acceleration term to give a modified density

$$\rho_m = \rho'(\text{effective density}) + \alpha(\text{centrifugal effect}) \qquad (2-16)$$

Substituting equations 2-15 and 2-16 into equation 2-14 yields

$$EIa^4 - (\rho'v^2 - T_p)a^2 + k = 0. \qquad (2-17)$$

The critical speed (V_{cr}) is the minimum speed that satisfies equation 2-17. Dr Clark[2] solves equation 2-17 by expressing the equation in terms of two parameters M and N. M is associated with the wave speed v and N is a single parameter representing the tire properties. M and

7

N have unique values associated with the critical speed (V_{cr}). The procedure for representing equation 2-17 in terms of M and N is as follows:

1. Let $N = \frac{EIa^4}{k}$ and $M = \frac{(\rho'v^2 - T_p)^2}{EIk}$

2. In terms of M and N, equation 2-17 may be rewritten as

$$N - \sqrt{MN} + 1 = 0. \tag{2-18}$$

3. Solving equation 2-18 for M gives

$$M = \frac{1}{N}(N+1)^2. \tag{2-19}$$

Because N is associated with the tire properties and M with the wave speed v, the minimum value of M satisfying equation 2-19 represents the unique value associated with the minimum speed (critical speed) satisfying the wave solution. The minimum value of M is obtained by solving for M in equation 2-19, differentiating with respect to N (the tire properties), setting the result equal to zero, solving for N, and substituting the value of N back into equation 2-19 to solve for the minimum value of M. It is found that the minimum value for M is 4.

To solve for the critical speed the value of 4 for M is substituted back into $M = \frac{(\rho'v^2 - T_p)^2}{EIk}$, and the equation solved for v, yielding

$$v = V_{cr}(\text{critical speed}) = \sqrt{\frac{T_p}{\rho'} + \sqrt{\frac{4kEI}{(\rho')^2}}}. \tag{2-20}$$

TIRE STRUCTURAL PROPERTIES

Modeling the tread band of bias and radial tires as a beam on an elastic foundation is common practice for studying tire vibrations. The challenge in applying this method to aircraft tires is correctly describing those terms used in the critical speed equation. The following paragraphs give a description of each term.

Bending Stiffness (EI)

A widely used material in the carcass of aircraft tires is 840/2 Nylon. The fabric modulus of elasticity (E_f) is the effective modulus in the longitudinal direction of the nylon-rubber ply laminate, and is a function of the cord half angle γ. Figure 2 is a plot of E_f versus γ obtained from 840/2 Nylon-rubber tensile tests conducted by Dr Clark[2].

The rubber tread modulus of elasticity (E_r) can vary from tire to tire and from manufacturer to manufacturer. The value of E_r is dependent on what compounds the manufacturer may use in the tread rubber. The tread will exhibit E_r values ranging from 500 psi to 2000 psi.

8
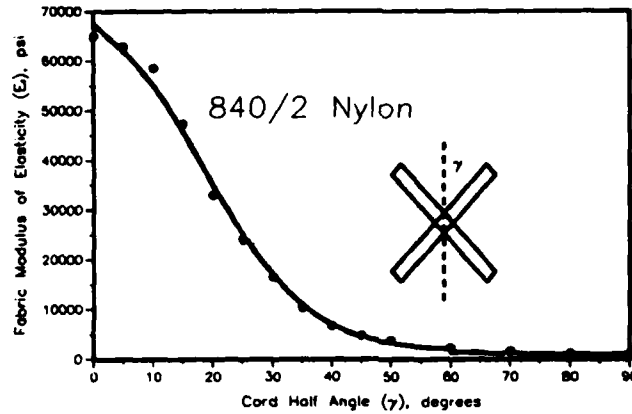
Figure 2. Fabric Modulus of Elasticity (E_f) versus Cord Half Angle (γ)

The bending stiffness (EI) is a function of E_f, E_r, the thickness of the rubber-tread region (t_r), and the thickness of the cord-rubber fabric region (t_f). Figure 3 shows a description of t_r and t_f. Bending stiffness (EI) can be expressed approximately as

$$EI = \frac{t_f^3 E_f}{12} + \frac{E_r}{4}[t_f^2 t_r + 2t_f t_r^2 + t_r^3] + \frac{E_r t_r^3}{12} \qquad (2-21)$$
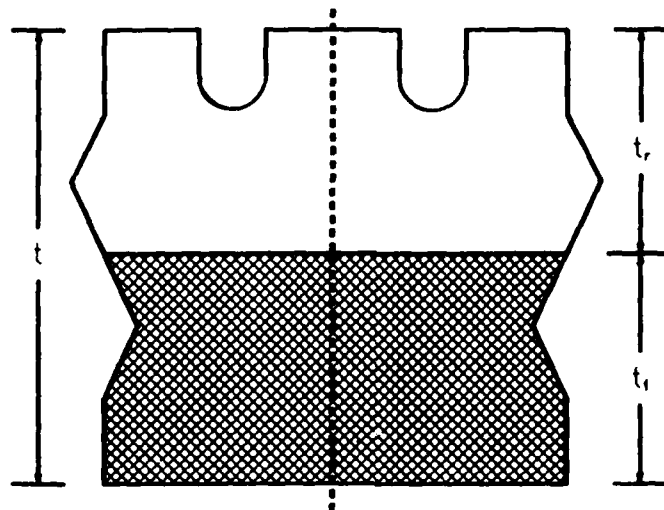
Figure 3. Tread cross-sectional parameters t_r and t_f

9

Linear Spring Constant (k)

The linear spring constant k describes the elastic restraints provided by the combined effect of the tire internal inflation pressure and sidewall. k relates a force per unit area to vertical tire deflection and is defined as

$$k = \frac{p_r}{d_r} \qquad (2-23)$$

where, p_r is the tire rated inflation pressure, and d_r is the rated tire deflection.

Belt Tension Due to Inflation Pressure (T_p)

The bias ply tire cross-sectional profile is idealized as the midline of the fabric structure as depicted by line O-A in Figure 4. Line O-A is divided into a tread region and sidewall region at the tire shoulder a-a. With the tire stationary, pressure forces are balanced by the carcass force F_c.

Referring to Figure 4 and taking moments about point O gives

$$F_c h = \frac{p_i h^2}{2} + \frac{p_i w_r^2}{2}. \qquad (2-23)$$

The tire section height (h) and w_r are related to an idealized cross-section radius of curvature (r) as

$$h = r(1 + \frac{\sqrt{2}}{2})$$
$$w_r = r\frac{\sqrt{2}}{2}$$

from which

$$w_r = \frac{\sqrt{2}h}{2 + \sqrt{2}}$$

Substituting for w_r into equation 2-23 and solving for F_c yields

$$F_c = 0.586 p_i h. \qquad (2-24)$$

The cord structure in a bias ply tire is illustrated in Figure 5. Let S be the collective cord load along the cord axis, l be the cord length, and γ be the cord half angle. In Figure 5, F_c and T_p are defined as

$$F_c = \frac{2S \sin\gamma}{l \cos\gamma} = \frac{2S \tan\gamma}{l} \qquad (2-25)$$

$$T_p = \frac{2S \cos\gamma}{l \sin\gamma} = \frac{2S \cot\gamma}{l} \qquad (2-26).$$

10
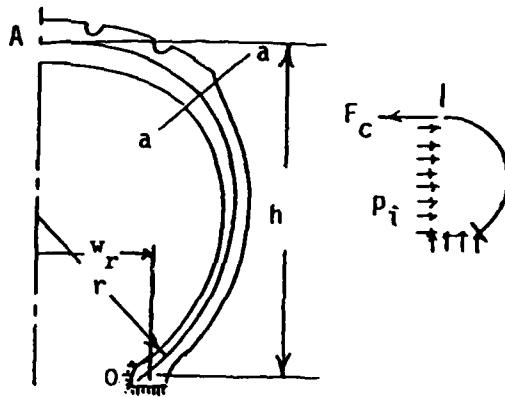
Figure 4. Idealized Shape Of the Bias Ply Tire Cross-Section
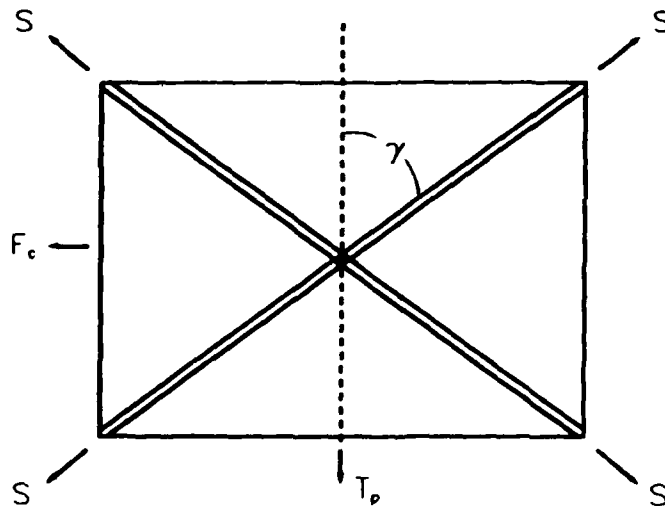
Figure 5. Cord Structure and Tensile Loads In a Bias Ply Tire

Combining equations 2-24 to 2-26 and rearranging gives the desired relation for the belt tension (T_p) as a function of inflation pressure, tire section height, and cord half angle.

$$T_p = 0.586 p_i h \cot^2 \gamma. \qquad (2-27)$$

Belt Tension Due to Centrifugal Effects (αv^2)

During rotation, the tire changes cross-sectional shape and grows to the shape depicted by line O-B in Figure 6. The horizontal carcass force F_c changes by an amount dF_c and the tread

11

centerline moves upward a distance dh. The new moment equilibrium equation about point O becomes

$$(F_c + dF_c)(h + dh) = \frac{p_i(h + d_h)^2}{2} + 0.0858p_ih^2 + Q(w_r - a)$$

where, Q is the centrifugal force equivalent to half the total centrifugal force acting on the cross-section, and a is the distance taken normal to the tire plane centerline from centerline to point of application of force Q. Retaining those terms associated with centrifugal effects and neglecting higher-order terms reduces the moment equilibrium equation due to centrifugal effects to

$$F_c dh + h dF_c = p_i h dh + Q(w_r - a). \qquad (2-28)$$

Recalling that $F_c = 0.586p_ih$, substituting for F_c into equation 2-28, and solving for dF_c yields

$$dF_c = 0.414p_i dh + \frac{Q(w_r - a)}{h}. \qquad (2-29)$$
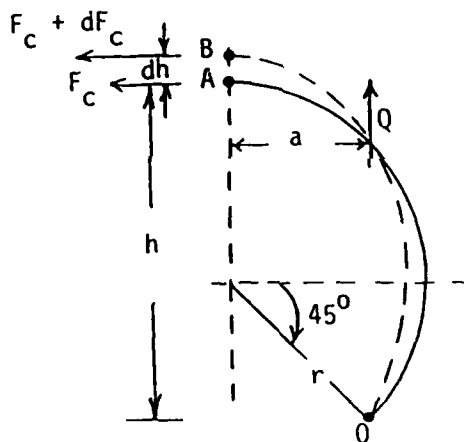
Figure 6. Change In Tire Cross-Sectional Shape During Rotation

Before equation 2-29 can be simplified to a usable form relations for Q, dh, and $(w_r - a)$ must be derived. In doing so, the overall cross-sectional shape is assumed to be circular as shown in Figure 7.

Defining ρ_1 as a mass per unit area of tire surface, then a differential mass element per unit width can be expressed as

$$dm = \rho_1 r d\theta.$$

A differential centrifugal force dQ can be expressed as

$$dQ = z\omega^2 dm$$
$$= z\omega^2 \rho_1 r d\theta$$

12

$$z = r(2 + \cos\theta)$$

$$x = r\sin\theta$$
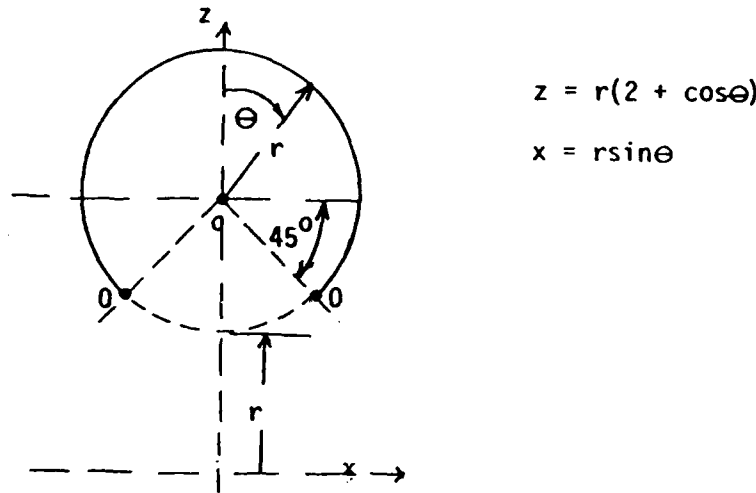
Figure 7. Circular Approximation to the Tire Cross-Sectional Shape

where ω is the tire rotational speed.

Integrating dQ from $0 \leq \theta \leq 3\pi/4$ gives a relation for Q as

$$
\begin{aligned}
Q &= \omega^2 \int_0^{\frac{3\pi}{4}} r(2 + \cos\theta)\rho_1 r\,d\theta \\
&= \rho_1 \omega^2 r^2 \frac{3\pi + \sqrt{2}}{2} \\
&= 5.42\rho_1 \omega^2 r^2.
\end{aligned}
\tag{2-30}
$$

It is more convenient to express Q in terms of the total tire mass m_t. It is assumed that the mass per unit surface area (ρ_1) is constant over the tire surface. The value of m_t is obtained by integrating ρ_1 over the tire surface as follows:

$$
\begin{aligned}
m_t &= \rho_1 \text{ (effective circumference)} \times \text{ (crosssectional profile arc length)} \\
&= \rho_1 \left[2\pi(\text{radial centroid } \bar{y})\right] \times \text{ (crosssectional profile arc length)} \\
&= \rho_1 \left[\frac{2\pi \int_0^{\frac{3\pi}{4}} r(2 + \cos\theta)r\,d\theta}{\int_0^{\frac{3\pi}{4}} r\,d\theta}\right] 2\int_0^{\frac{3\pi}{4}} r\,d\theta \\
&= 4\pi\rho_1 r^2 \int_0^{\frac{3\pi}{4}} (2 + \cos\theta)d\theta \\
&= 68\rho_1 r^2.
\end{aligned}
\tag{2-31}
$$

Solving equation 2-31 for ρ_1 and substituting the result into equation 2-30 leads to an expression for Q in terms of m_t which is expressed as

$$Q = 0.08 m_t \omega^2. \tag{2-32}$$

13

Referring to Figure 7 and taking moments of Q about the origin yields

$$M_o = \int x \, dQ$$

$$= \omega^2 \int_0^{\frac{3\pi}{4}} r(2 + \cos\theta)\rho_1 r^2 \sin\theta \, d\theta$$

$$= 3.66\rho_1\omega^2 r^3.$$

The distance a is given by

$$a = \frac{M_o}{Q}$$

$$= \frac{3.66\rho_1\omega^2 r^3}{5.42\rho_1\omega^2 r^2}$$

$$= 0.675r.$$

Recall that $w_r = \frac{r\sqrt{2}}{2}$, giving

$$wr - a = \frac{r\sqrt{2}}{2} - .675r$$

$$= 0.032r. \tag{2-33}$$

From the NASA Technical Report R-64[4] the radial growth (dh) due to centrifugal effects is expressed as

$$dh = \frac{0.01 m_t \omega^2}{p_i}. \tag{2-34}$$

Substituting equations 2-32 to 2-34 into equation 2-29 yields

$$dF_c = 0.00414 m_t \omega^2 + \frac{0.00256 m_t r \omega^2}{h}. \tag{2-35}$$

Noting that $h = r[1 + \sqrt{2}/2]$ and $W_t = m_t g$, equation 2-35 becomes

$$dF_c = 1.461 \times 10^{-5} W_t \omega^2 \tag{2-36}$$

where, W_t is the tire weight in pounds, and g is the gravitational constant, $386.1 in/s^2$.
From equations 2-25 and 2-26 the relation between dT and dF_c can be derived and expressed as

$$\frac{dT}{dF_c} = \cot^2\gamma. \tag{2-37}$$

Combining equations 2-36 and 2-37 and replacing ω^2 by $(v/r_o)^2$ leads to the following expression for the belt tension due to centrifugal effects,

$$dT = 1.461 \times 10^{-5} W_t \left(\frac{v\cot\gamma}{r_o}\right)^2 \tag{2-38}$$

$$= \alpha v^2$$

14

where,

$$r_o = \text{tire rolling radius}$$

$$\alpha = 1.461 \times 10^{-5} W_t \left(\frac{\cot \gamma}{r_o} \right)^2 \qquad (2-39)$$

Effective Tread Density (ρ')

The effective tread density (ρ') takes into account the average tread mass density (ρ_m) and centrifugal effects (α), and is expressed as

$$\rho' = \rho_m - \alpha.$$

The tread mass density (ρ_m) for a unit width of tread can be calculated from known specific weights of polymeric cord-rubber compounds of approximately 1.12 times that of water. The tread mass density as a function of tread thickness is

$$\rho_m = t \times 10^{-4}.$$

Subtracting the centrifugal effects (α) from the tread mass density leads to the effective density equation

$$\rho' = \left[t - 0.1461 W_t \left(\frac{\cot \gamma}{r_o} \right)^2 \right] \times 10^{-4}. \qquad (2-40)$$

CRITICAL SPEED (V_{cr}) FOR RATED CONDITIONS

A sample critical speed calculation is presented at rated conditions for a 49x17/26PR Type VII Goodyear tire, KC-135 main landing gear tire, Serial Number 51400054. Rated conditions are:

1. Deflection of approximately 29%
2. Vertical load of 39600 pounds
3. Inflation pressure of 170 psi
4. Maximum speed of 225 mph

The following paragraphs present calculations for the individual terms comprising the critical speed equation and the critical speed prediction.

Values for the fabric modulus of elasticity (E_f), rubber-tread modulus of elasticity (E_r), thickness of rubber-tread region (t_r), thickness of cord-rubber-fabric region (t_f), and cord half angle (γ) must be acquired before the bending stiffness (EI) can be calculated. Goodyear engineers suggested that a value of 38° be used for γ and a value of 2175 psi be used for E_r.

15

Knowing γ and referring to Figure 2, a value of E_f was determined to be 8571 psi. Values for t_r and t_f were 0.7 and 0.535 inches. EI is calculated as

$$EI = \frac{t_f^3 E_f}{12} + \frac{E_r}{4}[t_f^2 t_r + 2t_f t_r^2 + t_r^3] + \frac{t_r^3 E_r}{12}$$

$$= \frac{(0.535)^3(8571)}{12} + \frac{(2175)}{4}[(0.535)^2(0.7) + 2(0.535)(0.7)^2 + (0.7)^3] + \frac{(2175)(0.7)^3}{12}$$

$$= 752 \text{ lbs} - \text{in.}$$

The linear spring constant (k) is a function of the inflation pressure (p_i) and tire deflection (d). At rated conditions d is 29 percent of the section height (h), and is calculated to be 3.61 inches. The value of k is calculated as

$$k = \frac{p_r}{d_r}$$
$$= \frac{170}{3.61}$$
$$= 47.09 \ \frac{\text{lbs}}{\text{in}^3}.$$

The belt tension (T_p) due to inflation pressure is a function of inflation pressure (p_i), the tire section height (h), and cord half angle (γ). T_p is calculated as

$$T_p = 0.586 p_i h \cot^2 \gamma$$
$$= 0.586(170)(12.44)\cot^2(38^\circ)$$
$$= 2030 \text{ lbs/in.}$$

The effective density term (ρ') is a function of the tread thickness (t), tire weight (W_t), cord half angle (γ), and tire rolling radius (r_o). The tire weight at full tread depth was measured to be 187 pounds. r_o is defined as the tire undeflected outside radius minus one-third the tire deflection[4], and was calculated to be 22.98 inches. ρ' is calculated as

$$\rho' = \left[t - 0.1461 W_t \left(\frac{\cot \gamma}{r_o} \right)^2 \right] \times 10^{-4}$$

$$= \left[1.235 - .1461(187) \left(\frac{\cot(38^\circ)}{22.98} \right)^2 \right] \times 10^{-4}$$

$$= 1.150 \times 10^{-4} \ \frac{\text{lbs} - \text{s}^2}{\text{in}^3}.$$

16

The critical speed (V_{cr}) at rated conditions can now be calculated as

$$V_{cr} = \sqrt{\frac{T_p}{\rho'} + \sqrt{\frac{4kEI}{(\rho')^2}}}$$

$$= \sqrt{\frac{2030}{1.150 \times 10^{-4}} + \sqrt{\frac{4(47.09)(752)}{(1.150 \times 10^{-4})^2}}}$$

$$= 4574 \text{ in/s}$$

$$= 260 \text{ mph.}$$

SECTION III

PARAMETRIC STUDY

This section describes how critical speed changes with tire inflation pressure, cord half angle, tread depth, and aspect ratio. All results presented are for the 49x17/26PR Type VII Goodyear tire, Serial Number 51400054.

CRITICAL SPEED VERSUS INFLATION PRESSURE

Theory indicates that critical speed is most sensitive to belt tension due to tire inflation pressure. In practice, a common method to delay the speed at which the standing wave develops is simply to increase tire operational inflation pressure. Tire operational inflation pressures of modern aircraft and future aerospace vehicle concepts approach flotation and runway structural limitations. Consequently, increasing the tire operational inflation pressure to delay critical speed may not be a viable solution. Figure 8 shows the sensitivity of critical speed to tire inflation pressure. Tire deflection is kept constant while pressure and load are varied.

CRITICAL SPEED VERSUS CORD HALF ANGLE

The belt tension due to inflation pressure is also highly dependent on cord half angle. Small changes in this half angle will yield significant changes in belt tension, and in turn, critical speed. Therefore, the value for cord half angle in critical speed predictions should be precise. The value for this angle used in the critical speed equation is the cord half angle taken at the tire crown. Figure 9 shows the sensitivity of critical speed to cord half angle. Tire deflection, load, and pressure are at rated values.

CRITICAL SPEED VERSUS TREAD DEPTH

Changes in tread depth incur changes in tire aspect ratio, section height, and weight. These changes affect the values for bending stiffness, belt tension due to inflation pressure, and effective tread density. Changes in tread depth can have a significant effect on critical speed. A reduction in tread depth will delay critical speed to higher values. Table 1 lists the effects of tread depth on the terms of the critical speed equation and critical speed prediction. All calculations are done at rated conditions.

49x17/26PR Type VII Tire
Constant Deflection=2.61 inches

Variable Infl. Pressure and Load
Rated Max Speed = 225 mph
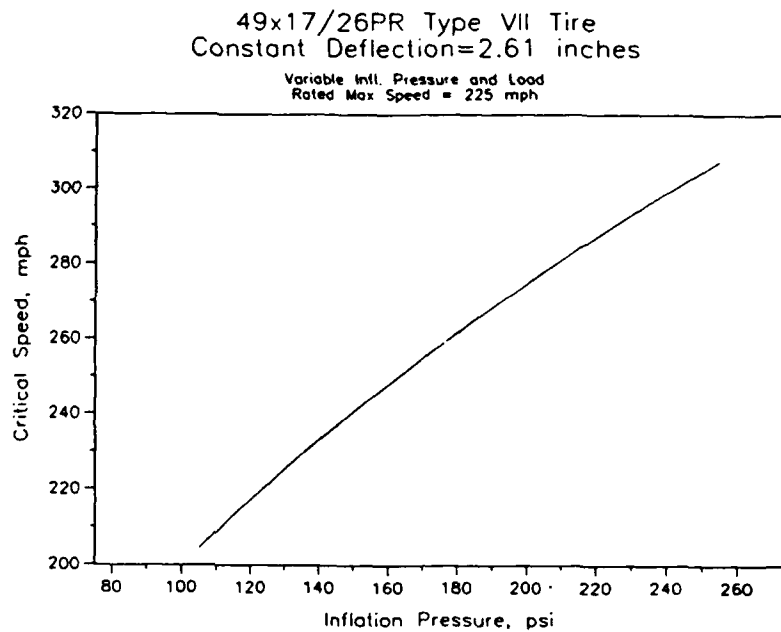
Figure 8. Critical Speed versus Inflation Pressure, 49x17/26PR Type VII Tire

49x17/26PR Type VII Tire
Rated Conditions

Rated Maximum Speed = 225 mph
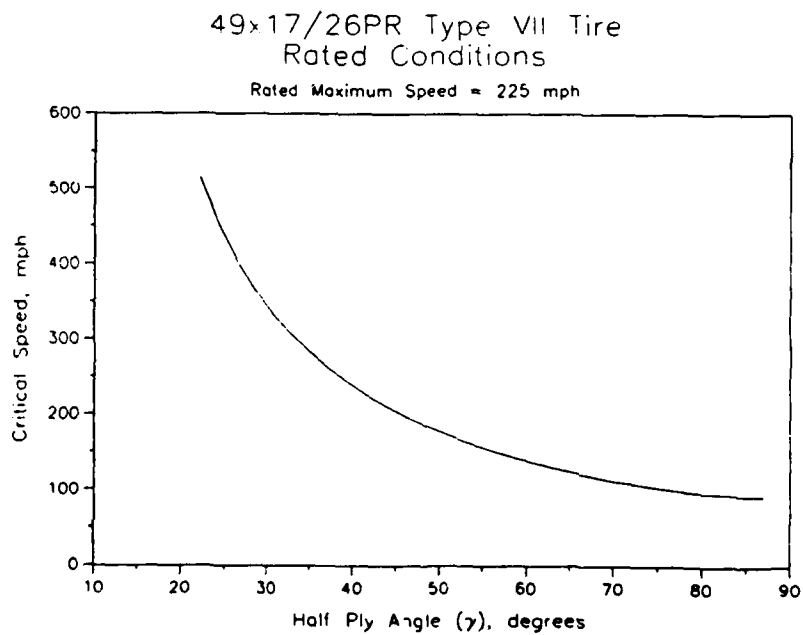
Figure 9. Critical Speed versus Cord Half Angle, 49x17/26PR Type VII Tire

19

TABLE 1. THE EFFECT OF TREAD DEPTH ON CRITICAL SPEED FOR A 49x17/26PR TYPE VII GOODYEAR TIRE, RATED CONDITIONS.

t	t_r	h	EI	W_t	$\rho' \times 10^4$	T_p	V_{cr}
1.235	0.700	12.44	752	187	1.150	2030	260
1.048	0.513	12.25	415	178	0.966	2000	276
0.844	0.309	12.05	229	166	0.766	1966	303
0.635	0.100	11.84	131	151	0.563	1932	346

where,

t = total tread thickness, inches

t_r = rubber − tread depth, inches

h = tire section height, inches

EI = bending stiffness, lbs − in

W_t = tire weight, pounds

ρ' = effective tread density, lbs − s^2/in^3

T_p = belt tension due to inflation pressure, lbs/in

V_{cr} = critical speed, mph.

CRITICAL SPEED VERSUS TIRE ASPECT RATIO

The tire aspect ratio (A_R) is a geometric parameter defined by the ratio of section height (h) to section width (w_s). A_R can be expressed as

$$A_R = \frac{h}{w_s} = \frac{D_o - D}{2w_s} \qquad (3-1)$$

where,

D_o = tire outside diameter

D = wheel rim ledge diameter + (2 × flange height).

For this analysis, variations in tire aspect ratio are due to changes in section height while maintaining a constant section width. Tire percent deflection and vertical loads are kept constant. As a result, rated inflation pressure, vertical stiffness, and outside diameter must be adjusted. To estimate these adjustments a load/deflection relation for Type VII bias ply tires[4] was utilized. The relation is expressed as

$$F_z = 2.4w_s(p_i + 0.08p_r)\sqrt{(w_s D_o)}\left(\frac{d}{w_s} - C_z\left[1 - e^{(-0.6d/w_s)/C_z}\right]\right) \qquad (3-2)$$

20

where,

$$F_z = \text{vertical load, pounds}$$

$$p_i = \text{inflation pressure, psi}$$

$$p_r = \text{rated inflation pressure, psi}$$

$$w_s = \text{cross} - \text{sectional width, inches}$$

$$D_o = \text{outside tire diameter, inches}$$

$$d = \text{tire deflection, inches}$$

$$C_z = \text{empirical constant, approximately } 0.03.$$

When considering only rated conditions (i.e., $p_i = p_r$) and using equation 3-1, then equation 3-2 can be expressed in terms of the tire aspect ratio as

$$F_z = 2.592 p_r w_s \sqrt{w_s(2w_s A_R + D)} \left(\frac{d}{w_s} - C_z \left[1 - e^{(-0.6d/w_s)/C_z} \right] \right) \qquad (3-3)$$

The tire vertical stiffness (K_z) is obtained by taking the derivative of equation 3-3 with respect to tire deflection, yielding

$$K_z = 2.592 p_r \sqrt{w_s(2w_s A_R + D)} \left[1 - 0.6 e^{(-0.6d/w_s)/C_z} \right] \qquad (3-4)$$

The desired expression for K_z is obtained by solving equation 3-4 for p_r, substituting the result into equation 3-3, and rearranging. This leads to an expression for K_z given by

$$K_z = \frac{F_z}{w_s} \frac{1 - 0.6 e^{(-0.6d/w_s)/C_z}}{\frac{d}{w_s} - C_z \left[1 - e^{(-0.6d/w_s)/C_z} \right]} \qquad (3-5)$$

The 49x17/26PR Type VII Goodyear tire is used as a baseline defining constant values for rated load, percent deflection, and section width. A section width (w_s) of 16.92 inches was measured for the subject tire. By fitting equation 3-2 to experimental load/deflection data a value of 0.0337 for C_z was obtained. D for the 49x17/26PR tire is 23.5 inches. For rated load $(F_z = 39600 \text{ lbs})$ and percent deflection (29%), the data in Table 2 was generated along with calculated critical speeds using equations 2-20, 3-1, 3-3, and 3-5.

TABLE 2. THE EFFECT OF TIRE ASPECT RATIO ON CRITICAL SPEED FOR A 49x17/26PR TYPE VII GOODYEAR TIRE AS A BASELINE, RATED CONDITIONS.

A_r	h (inches)	D_o (inches)	d (inches)	K_z (lbs/in)	p_r (psi)	V_{cr} (mph)
1.0	16.92	57.34	4.91	9087	113	236
0.9	15.23	53.96	4.42	10213	131	243
0.8	13.54	50.57	3.93	11642	155	252
0.7	11.84	47.19	3.43	13653	189	263
0.6	10.15	43.80	2.94	16080	234	275
0.5	8.46	40.42	2.45	19654	304	292

21

The data of Table 2 indicate that tire aspect ratio has a significant effect on critical speed. By maintaining constant section width for variations in tire aspect ratio, the values of section height and inflation pressure must be adjusted for a given rated load and percent deflection. Both section height and inflation pressure contribute to the belt tension due to inflation pressure; belt tension having the greatest influence on critical speed. Again, tire operational inflation pressure limits may dictate a lowest practical tire aspect ratio.

SECTION IV

VALIDATION

This section describes the tests conducted to provide full-scale tire laboratory data for validation of the analytical techniques used in predicting critical speed. The KC-135 49X17, 26 ply rating, tire was used as a baseline to establish dynamometer test methodology for high speed operational assessment (inertia effects/critical speed) of current tire design limitations. This tire size was selected as the baseline because of its availability, high-speed (224 MPH), and high-load (39,600 lbs) capability.

TEST MATRIX

A detailed test matrix, Table A-1, Appendix , was prepared to establish the critical speed (V_{cr}) limitations of the baseline 49X17 tire at various test conditions.

Test series 1P&L through 6P&L, and 14P&L through 16 P&L were to be conducted at constant load (39600 lbs. flat plate and rated) to determine the effect of pressure, deflection, and mold skid depth on critical speed. The mold skid depth or the groove depth is defined as the thickness of tread between the tire's outer tread surface and the bottom of the tread groove.

Test series 4P&L, 5P&L, 7P&L through 11P&L, and 17P&L through 19P&L were to be conducted at rated deflection (170 PSI inflation pressure and 39600 LBS flat plate and rated load) to determine the effect of pressure load and mold skid depth on critical speed.

Test series 4P&L, 5P&L, 12P&L, and 17P&L through 31P&L were to be conducted at constant pressure to determine the effect of load and deflection on critical speed.

TEST METHOD

All critical speed tests were conducted in the AFWAL Landing Gear Development Facility using the 120-inch programmable dynamometer. The 49X17/26PR tires were taken from the same manufacturer (Goodyear), production lot (serial numbers 50280284 through 53570337), and qualification (QTR 461B-2049-TL). In each of the 62 test series listed in the Test Matrix, a different 49X17/26PR test tire was to be used.

Tire Preparation and Break-in

All test tires were subjected to a 12 hour stretch and a 24-hour air-retention check in accordance with MIL-T-5041 [5]. The rated inflation pressure of 170 PSI was used. Tires were buffed to the specified mold skid depth (0.10 or 0.30 inches) as applicable per the Test Matrix. Tires were buffed uniformly across the full width of the tread by Air Treads, Inc. After buffing, new weight and unbalance data were obtained. Each test tire was conditioned by conducting a taxi roll on the dynamometer for 2 miles at 39600 LBS rated load and at 30 MPH constant speed.

Test Procedure

Correction for flywheel curvature was accomplished by pressure adjustment for test series 1P through 31P. At the specified flat plate inflation pressure, the correction for flywheel curvature was made by increasing the pressure to obtain the desired deflection. Flat plate and flywheel tire deflection data was obtained.

Correction for flywheel curvature was accomplished by load adjustment for test series 1L through 31L. At the specified flat plate inflation pressure, the correction for flywheel curvature was made by reducing the load on the flywheel to obtain the desired deflection. Flat plate and flywheel tire deflection data was obtained.

Correction for flywheel curvature by load reduction is the preferred adjustment in lieu of pressure increase. Pressure increase results in a much higher critical speed, in some cases far exceeding the rated speed of the tire. Thus, premature failures due to tread rotational inertia and adhesion limitations are likely to occur before critical speed is reached as predicted.

Initially, the first test velocity listed in each test series was approximately 20 percent lower than the calculated V_{cr} value. As the confidence level increased with the use of the V_{cr} prediction techniques, the first test velocity was set approximately 10 percent lower than the calculated value. Subsequent test cycles were performed by increasing the test velocity in increments of either 5 or 10 MPH until the critical speed was reached. Once V_{cr} was reached, testing was continued until tire failure occurred. Each test cycle was recorded on videotape.

To prevent tire slippage during spin-up on the dynamometer, the tire was lightly loaded against the stationary flywheel. Then the flywheel was brought up to the test velocity using maximum acceleration and the tire was further loaded to the specified test load.

For each test cycle, at the specified constant normal load, the velocity was held at steady-state for a limited duration. At the end of the test cycle, the tire was unloaded from the flywheel and the contained air temperature was allowed to cool to $75 \pm 10°$ F before proceeding to the next higher velocity increment. The test duration was initially set at 3 seconds per cycle, but

24

was considered too short a time duration to visually observe tire deformation at V_{cr}. The test duration was then doubled, but the 6-second duration resulted in the entire tread stripping resulting in damage to the test equipment. Finally, a 4-second test duration was adopted and used throughout the remaining tests.

A painted grid on the tire's sidewall was used on the first few tires tested. This approach was terminated since there was no visual evidence of deformation in the sidewall during V_{cr}.

TEST RESULTS

A series of dynamometer tests were conducted to validate the predicted V_{cr} trends including the effects of inflation pressure, mold skid depth, normal load, and deflection. A limited number of V_{cr} test series, as specified in the Test Matrix, have been conducted on the 49X17/26PR baseline tire.

Results of the V_{cr} tests to date are summarized in Table 3. As shown in this table, the predicted V_{cr} values are very near the experimental values, within +13.3 percent and -1.5 percent with an average of 2.9 percent.

In evaluating the baseline tire's test results, the following trends were observed based on the limited tests performed:

Effect Of Inflation Pressure

Trend data in terms of V_{cr} versus inflation pressure is shown in Figure 10. Results show that the predicted (V_{cr-p}) and experimental (V_{cr-e}) critical speeds increased significantly as the inflation pressure is increased. As illustrated in this figure, this trend holds true for the three different mold skid depth levels investigated. Each data point in the figure represents a separate test tire in a given test series.

As observed from Figure 10, the critical speed values predicted from the analytical model are in good agreement with the experimental values. Even over the wide pressure (102 to 197 PSI) range and mold skid depth (0.125 to 0.53 inches) range, there is generally good agreement between V_{cr-e} and V_{cr-p} results.

TABLE 3. CRITICAL SPEED COMPARISONS: PREDICTED $(V_{cr\ p})$ VERSUS EXPERIMENTAL $(V_{cr\ e})$.

TIRE	TEST SERIES	PRESS. (psi)	% DEFL.	LOAD (lbs)	V_{cr-p} (mph)	V_{cr-e} (mph)	% DIFF.
a) Full Tread Depth (0.47 to 0.53 inches)							
2-N	1P	125	48.3	39600	217	210	3.3
3-N	1P	125	48.0	39600	218	215	1.4
4-N	1L	102	42.5	31500	197	200	-1.5
4-N	1L	102	42.5	31500	197	200	-1.5
5-N	4P	197	28.9	39600	272	240	13.3
6-N	4P	197	28.5	39600	275	245	12.2
12-N	4L	170	29.7	34500	254	*	—
20-N	7P	125	29.6	25700	222	220	0.9
19-N	7L	102	29.7	21900	202	205	1.5
21-N	12P	197	20.0	24700	278	*	—
29-N	17L	136	28.9	28000	234	*	—
31-N	20L	136	20.0	18000	236	240	-1.5
32-N	14L	136	34.2	34000	231	*	—
33-N	26L	102	20.0	14500	204	215	5.1
34-N	4L	170	28.5	34500	255	245	4.1
38-N	12L	170	20.0	22300	261	260	0.4
40-N	14L	136	33.8	33600	231	*	—
41-N	17L	136	28.7	27500	230	*	—

Notes: * Tread failure occurred prior to an onset of the standing wave.

** No standing wave was observed at this low (10%) tire deflection.

TABLE 3. (CONCLUDED)

TIRE	TEST SERIES	PRESS. (psi)	% DEFL.	LOAD (lbs)	V_{cr-p} (mph)	V_{cr-e} (mph)	% DIFF.
			b) Intermediate Tread Depth (0.31 to 0.34 inches)				
7-N	2P	125	48.5	39600	232	230	2.7
8-N	2P	125	48.3	39600	231	225	2.7
9-N	2L	102	41.8	33300	211	210	0.5
10-N	8P	119	29.0	25000	230	225	2.2
11-N	8L	102	29.7	21900	212	210	1.0
13-N	15P	158	33.8	39600	262	*	–
14-N	15L	136	34.4	33900	246	235	4.7
17-N	18L	136	28.3	27800	248	240	3.3
16-N	21L	136	20.0	18500	248	250	-0.8
18-N	24L	136	10.0	7700	255	**	–
42-N	27L	102	20.0	13000	220	225	-2.3
			c) Shallow Tread Depth (0.09 to 0.14 inches)				
22-N	3L	102	42.4	34000	222	225	-1.2
23-N	9L	102	29.3	22100	234	225	4.0
24-N	19L	136	28.9	27830	268	265	1.1
25-N	16L	136	33.9	34000	270	270	0
26-N	22L	136	20.0	18000	274	270	1.5
28-N	28L	102	20.0	14000	237	245	3.3
27-N	3P	125	42.2	39600	261	*	–

Notes: * Tread failure occurred prior to an onset of the standing wave.

      ** No standing wave was observed at this low (10%) tire deflection.
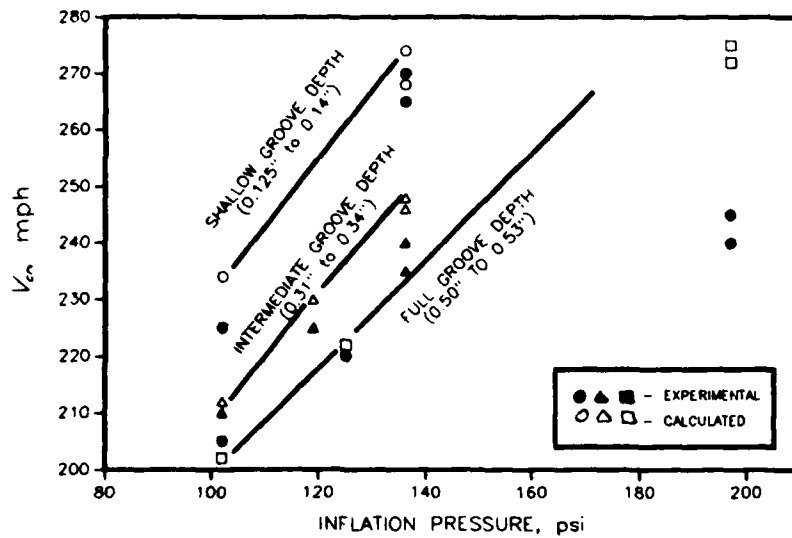
Figure 10. V_{cr} versus Inflation Pressure for the Various Mold Skid Depths. Normal Deflection Range (28% to 34%)
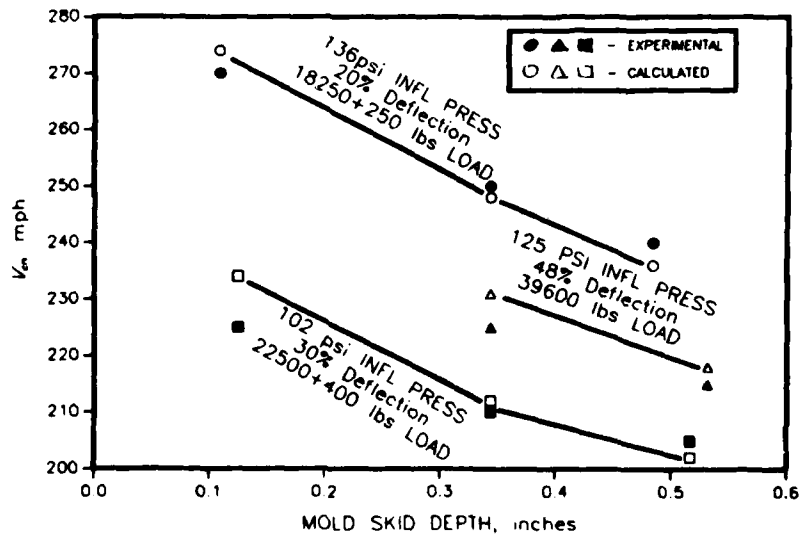
Figure 11. V_{cr} versus Mold Skid Depth for Various Inflation Pressure and Load Combinations

28

Effect Of Mold Skid Depth

Trend data in terms of V_{cr} versus mold skid depth is shown in Figure 11 for various inflation pressure and load combinations. Both experimental and predicted results showed that as the tire's mold skid depth is reduced, the critical speed increases significantly. Again, there is relatively good agreement between the predicted and experimental results.

For the shallow mold skid depth of 0.11 to 0.14 inches a standing wave occurs in the shoulder region approximately 5 to 25 MPH sooner than the onset of the standing wave in the tread region. The higher the tire's operating deflection, the greater the speed differential of a standing wave occurring between the shoulder and the tread. For example, at 42 percent tire deflection (test series 3L), standing waves occurred at 200 MPH in the shoulder region and at 225 MPH in the tread region, a differential of 25 MPH. However, at the lower tire deflection of 20 percent (test series 22L) the speed differential was only 5 MPH.

Effect Of Normal Load

Trend data in terms of V_{cr} versus normal load is shown in Figures 12 and 13. Both predicted and experimental values showed that changes in the tire's normal load had little influence on the tire's critical speed. This trend holds true for the baseline tire at other inflation pressure conditions as well as for the different mold skid depths investigated.

Effect Of Tire Deflection

Trend data in terms of V_{cr} versus tire deflection is shown in Figures 14 and 15. Both predicted and experimental results showed that changes in percent deflection had an insignificant impact on the baseline tire's critical speed. This trend holds true for the baseline tire at the three different mold skid depth levels as well as for the various inflation pressures investigated to date. A typical comparison of experimental and predicted V_{cr} (using an expanded scale) is illustrated in Figure 15 for the baseline tire at 136 PSI inflation pressure, intermediate groove depths, and over a 20 to 34 percent deflection range. There is good agreement between the predicted and experimental results, with differences ranging between +0.8 and -4.7 percent for this one set of conditions. This comparison is typical for all conditions.

Failure Mode/Location.

Failure mode and failure location are dependent on mold skid depth, test duration, tire deflection, and predicted critical speed. The predominant failure mode during V_{cr} tests was

29
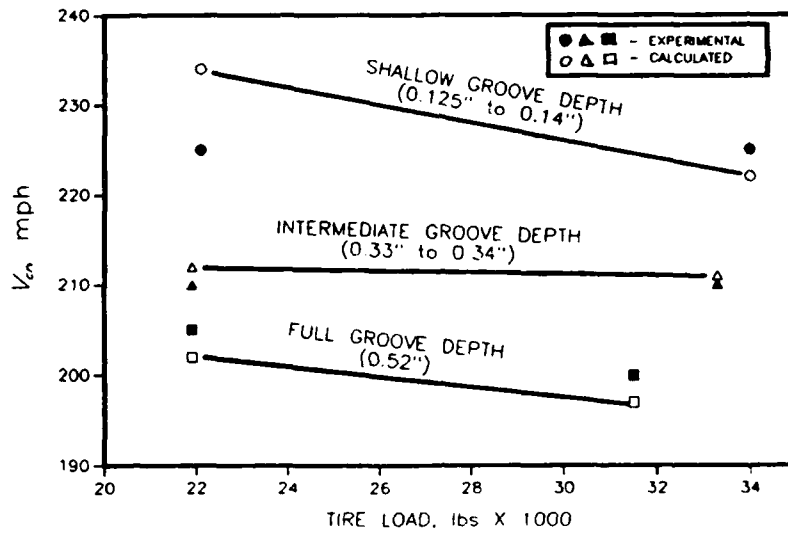
a) 102 psi Inflation Pressure (0.6 × Rated)
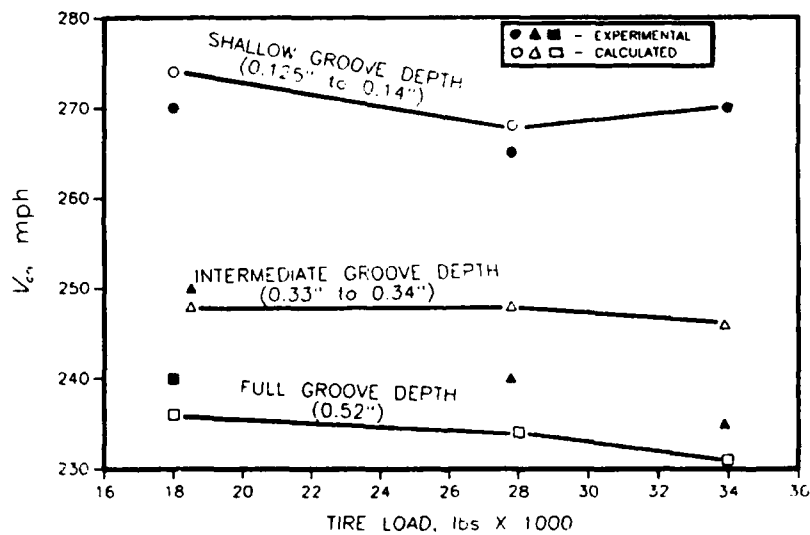
b) 136 psi Inflation Pressure (0.8 × Rated)

Figure 12. V_{cr} versus Tire Load at Two Inflation Pressures

30
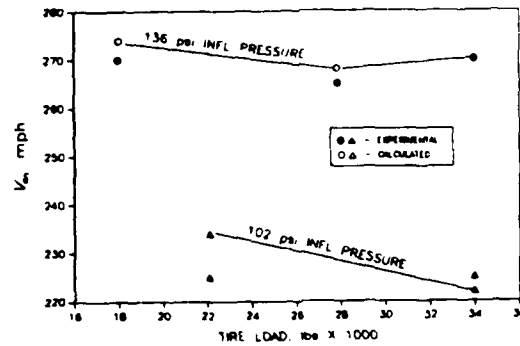
a) Shallow Groove Depth (0.11 to 0.14 inches)
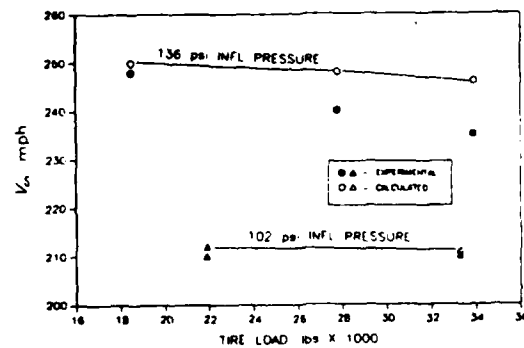
b) Intermediate Groove Depth (0.31 to 0.34 inches)
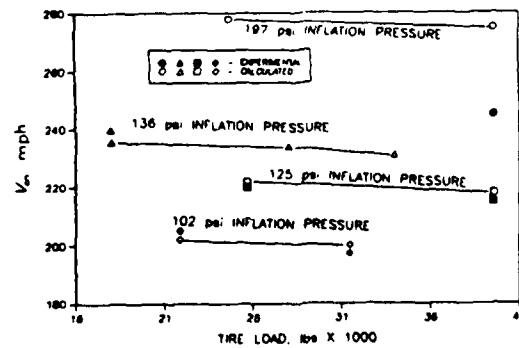
c) Full Groove Depth (0.47 to 0.53 inches)

Figure 13. V_{cr} versus Tire Load for Various Groove Depths

31
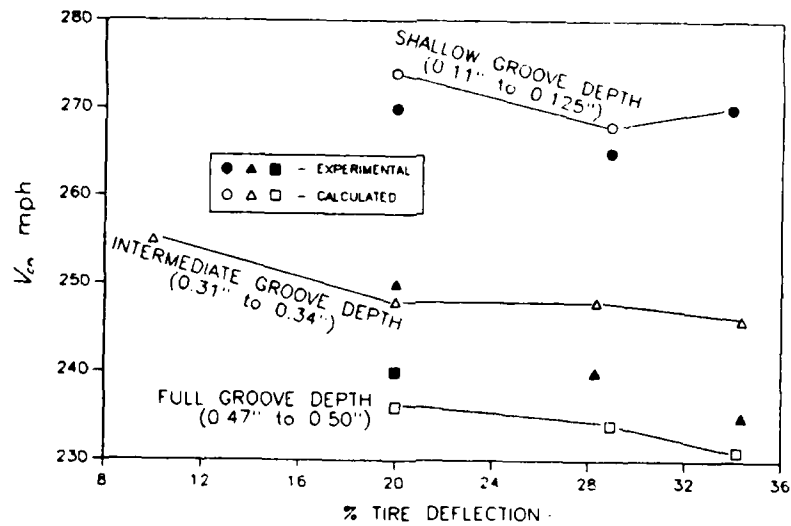
Figure 14. V_{cr} versus Percent Deflection for $49 \times 17/26$PR Tire at 136 psi Inflation Pressure for the Various Mold Skid Depths
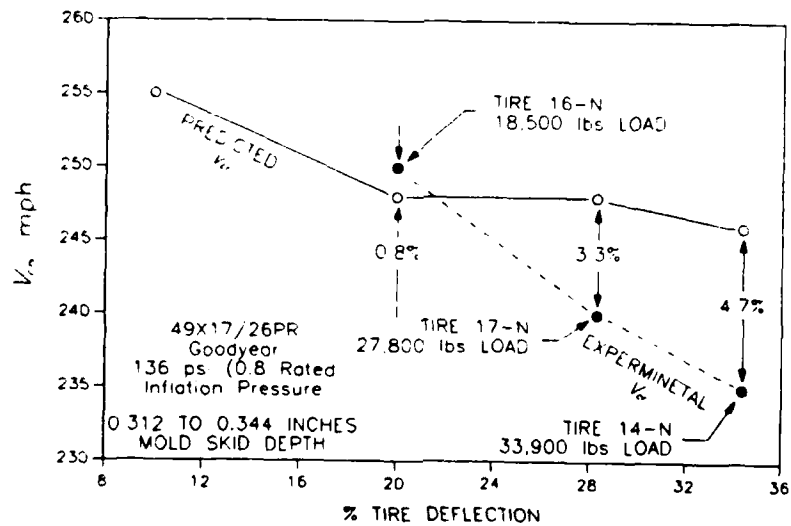
Figure 15. V_{cr} versus Percent Deflection for 136 psi Inflation Pressure and 0.328 ($\pm$ 0.12) inches Mold Skid Depth

32

tread separation. Initially, groove cracking was observed, then progressed to tread undercutting and subsequent tread chunking.

All failures that occurred on tires at full mold skid depth (0.52 inches) were due to tread chunking in the center rib. In 4 of the test series (4L, 12P, 14L and 17L), tires at the full mold skid depth failed prematurely before reaching the predicted V_{cr}. A typical failure at full mold skid depth is shown in Figure 16.

Groove cracking appeared at the outer grooves when operating at higher deflections (40 percent range) for an intermediate mold skid depth of 0.3 inches, test series 2P and 2L (Figure 17). The failure location would shift toward the center rib and tread chunking would occur when operating in the normal deflection range (20 to 33 percent), test series 8L, 15P, 15L (Figure 18), 18L and 21L. No visible failure occurred when operating at 10 percent deflection (test series 24L). Also, there was no indication of V_{cr} when operating at this low deflection.

For the shallow mold skid depth of 0.1 inches, tread chunking would occur at the shoulder ribs when the predicted critical speed was low, (222 MPH test series 3L to 234 MPH in test series 9L). However, when the predicted V_{cr} was high, (268 MPH in test series 19L, 270 MPH in test series 16L and 274 MPH in test series 22L), the tread chunking failure location shifted to the center rib.

The most severe tread chunking occurred during the longest test duration used (6 seconds). In test series 1P and 4P, the entire tread stripped during the 6-second duration of the first cycle on each tire (tire code 3-N and 6-N, respectively). As previously discussed under the Test Method subsection, a 4-second test duration was adopted and used throughout the remaining tests.

Experimental V_{cr} Criteria

The most successful method used in determining the occurrence of a standing wave in the tread band is to visually observe its inception. Tread elements transition from the tire footprint to a free rolling radius through a smooth radius of curvature for speeds well below V_{cr}. The transition radius of curvature decreases significantly as V_{cr} is approached. This is exhibited by the tread elements growing into the flywheel and is consider the inception of the standing wave. Radial displacement of the tread continues to increase with speed and propagate along the tire circumference in the sinusoidal fashion. The speed associated with the standing wave inception is V_{cr}. This method proved to be acceptable for tire deflections above 20 percent. Because of the low displacement amplitudes at tire deflections less than 20 percent, it was difficult to the inception of the standing wave. Large increases in drag force and rolling resistance, were not observed at critical speed in most test cases as originally expected. One good example where

33

drag force suddenly Increased at critical speed Is In test series 15L (test tire code 14-N). The Inception of a standing wave In this test series was first noticed at 235 MPH. At 240 MPH, the minimum and maximum drag force values Increased by 385 and 194 percent respectively, and the maximum rolling resistance had Increased by 180 percent over those values of the previous test run.

An Increase In noise level was usually accompanied with a visual detection of the standing wave, indicating the Initial stages of failure, i.e., tread chunking and tread stripping. However, an Increase In noise level Is not solely a positive Indicator of critical speed. Increases In noise level can also occur when tires fail prematurely (prior to reaching V_{cr}) or after exceeding the V_{cr} and then failing at higher speeds.

Repeatability of results between two tires was demonstrated In test series 1P and 4P. In test series 1P, tires 2-N and 3-N had predicted critical speeds of 217 and 218 MPH, respectively, and experimental critical speeds of 210 and 215 MPH, respectively. In test series 4P, tires 5-N and 6-N had predicted critical speeds of 272 and 275 MPH, respectively, and experimental critical speeds of 240 and 245 MPH, respectively.

Repeatability of results with one tire was also demonstrated using tire 2-N In test series 1P. The onset of a standing wave was observed In two separate test runs on this tire at a critical speed of 210 MPH, prior to tread failure.

34

S/O No 87-1

SIZE 49x17   PR 26

MANUFACTURER   GOODYEAR

SERIAL No 50280300   CODE 12-N

TEST SERIES 4L   TEST DATE 6 MAY 87

TYPE OF FAILURE TREAD CHUNKING

IN CENTER RIB, 6 IN.

**Figure 16. Typical Tread Failure at Center Rib. Full Mold
Skid Depth. Tire Code 12-N, Test Series 4L.**

S/O No 87-1

SIZE 49x17   PR 26

MANUFACTURER GOODYEAR

SERIAL No 52490287   CODE 9-N

TEST SERIES 2L   TEST DATE 15-18 MAY 87

TYPE OF FAILURE: TREAD CHUNKING IN OB
SHOULDER + 2 E SHOULDER RIB

b) Tread Chunking and Groove Cracking in Outboard Rib.

**Figure 17. Typical Tread Failure at Outboard Rib. Intermediate Mold
Skid Depth. 41.8% Tire Deflection. Tire Code 9-N, Test Series 2L.**

a) Close-up of Groove Cracks.
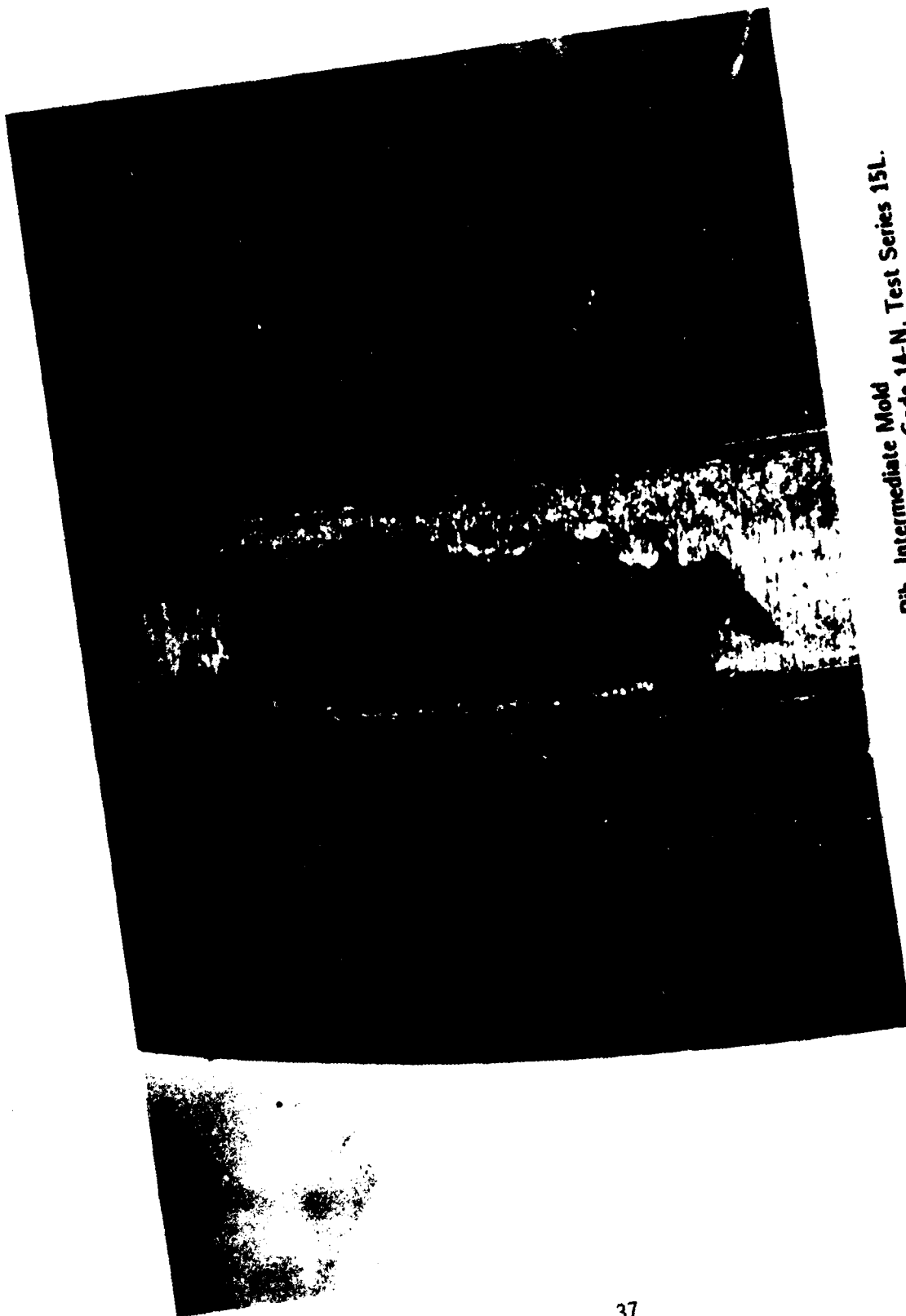
Figure 18. Tread Failure at Center Rib. Intermediate Mold Skid Depth. 34.4% Tire Deflection. Tire Code 14-N. Test Series 15L.

37

SECTION V

CONCLUSIONS
AND
RECOMMENDATIONS

1. Both the analytical and experimental results showed that the major parameters affecting critical speed are inflation pressure and mold skid depth. Changes in normal load and in percent deflection had little influence on the tire's critical speed.

2. The critical speed values predicted from the analytical model are in good agreement with the experimental values observed during the initial tests on the baseline tire.

3. Alternate methods should be explored for the detection of the standing wave. The visual cue used during this study is subjective and does not represent a definitive indication of the onset of a standing wave.

4. Other causes such as purely centrifugal effects may account for tread retention failure prior to the onset of a standing wave. These types of failure were observed to take place at inflation pressures equal to or greater than rated inflation pressure and with full mold skid depth.

5. Critical speed is sensitive to the crown cord half angle. For this reason, an accurate value for the crown cord half angle should be used for quantitative prediction purposes.

6. Baseline tires from another vendor (B.F.Goodrich), other tire sizes (25.5x8.0-14/18PR/250 MPH and 34.5x9.75-18/26PR/259 MPH), and the radial tire should be included in the critical speed study.

38

REFERENCES

1. **Theory and Analysis of Flight Structures**, Robert M. Rivello, University of Maryland, 1969, pp. 98-177.

2. **Technology Needs for High Velocity Vehicle Aircraft Tires**, S.K. Clark, Precision Measurement Company, February 1987.

3. **Tire Vibration**, G.R. Potts, C.A. Bell, L.T. Charek and T.K. Roy, Tire Science and Technology, TSTCA, Vol. 5, No. 4, Nov. 1977, pp. 202-225.

4. **NASA-TR-R-64**, Mechanical Properties of Pneumatic Tires with Special Reference to Modern Aircraft Tires, R.F. Smiley and W.B. Horne, Langley Research Center, 1960.

5. **MIL-T-5041G**, Military Specification—Tires, Pneumatic, Aircraft, 12 September 1975.

APPENDIX

TEST MATRIX — CRITICAL SPEED 49 × 17/26PR, TYPE VII, TIRE.

TABLE A-1

TEST CYCLE NR.	TEST VEL. (mph)	GROOVE DEPTH (Inches)	INFLATION PRESSURE (psi)	NORMAL LOAD (lbs)	TEST DEFL.
1P160	160	0.52	102 psi	39600	= F.P. DEFL
1P170	170	(FULL)	(F.P.),		@ 102 psi &
1P180	180		ADJUST		39600 lbs
1P...*	...*		PRESS		LOAD
1PV_{cr}	V_{cr}		FOR F.W. CURVA-		
2P180	180	0.30	TURE		
2P...*	...*				
2PV_{cr}	V_{cr}				
3P200	200	0.10			
3P...*	...*				
3PV_{cr}	V_{cr}				
1L160	160	0.52	102 psi	39600 lbs	= F.P. DEFL
1L170	170	(FULL)		(F.P.),	@ 102 psi &
1L180	180			ADJUST	39600 lbs
1L...*	...*			LOAD	LOAD
1LV_{cr}	V_{cr}			FOR F.W. CURVA-	
2L180	180	0.30		TURE	
2L...*	...*				
2LV_{cr}	V_{cr}				
3L200	200	0.10			
3L...*	...*				
3LV_{cr}	V_{cr}				

NOTES:
* Continue to increase the test speed in increments of 5 or 10 mph in subsequent test cycles until the critical speed (V_{cr}) is reached.
(1) F.P. - flat plate, F.W. - flywheel
(2) The second character in the test cycle number identifies the method taken to compensate for flywheel curvature, either by pressure ("P") increase or by load ("L") reduction.
(3) All approximations ($\approx$) were obtained from load-deflection curves, Goodyear report QTR 461B-2049-TL, 49x17/26PR tire.
(4) Groove depth.- the mold skid depth or the groove depth after buffing.

TABLE A-1. (CONTINUED)

TEST CYCLE NR.	TEST VEL. (mph)	GROOVE DEPTH (Inches)	INFLATION PRESSURE (psi)	NORMAL LOAD (lbs)	TEST DEFL.
4P210	210	0.52	170 psi (F.P.),	39600 lbs	= F.P. DEFL
4P220	220	(FULL)	ADJUST		@ 170 psi
4P230	230		PRESS		39600 lbs
4P...*	...*		FOR F.W.		LOAD
$4PV_{cr}$	V_{cr}		CURVA-TURE		
5P230	230	0.30			
5P...*	...*				
$5PV_{cr}$	V_{cr}				
6P230	230	0.52	204 psi (F.P.)		= F.P. DEFL
6P240	240	(FULL)	ADJUST		@ 204 psi &
6P250	250		PRESS		39600 lbs
6P...*	...*		FOR F.W.		LOAD
$6PV_{cr}$	V_{cr}		CURVA-TURE		
4L210	210	0.52	170 psi	39600 lbs (F.P.),	= F.P. DEFL
4L220	220	(FULL)		ADJUST	@ 170 PSI &
4L230	230			LOAD	39600 lbs
4L...*	...*			FOR F.W.	LOAD
$4LV_{cr}$	V_{cr}			CURVA-TURE	
5L230	230	0.30			
5L...*	...*				
$5LV_{cr}$	V_{cr}				
6L230	230	0.52	204 psi	39600 lbs (F.P.),	= F.P. DEFL
6L240	240	(FULL)		ADJUST	@ 204 psi &
6L250	250			LOAD	39600 lbs
6L...*	...*			FOR F.W.	LOAD
$6LV_{cr}$	V_{cr}			CURVA-TURE	

NOTES:

* Continue to increase the test speed in increments of 5 or 10 mph in subsequent test cycles until the critical speed (V_{cr}) is reached.

(1) F.P. - flat plate, F.W. - flywheel

(2) The second character in the test cycle number identifies the method taken to compensate for flywheel curvature, either by pressure ("P") increase or by load ("L") reduction.

(3) All approximations ($\approx$) were obtained from load-deflection curves, Goodyear report QTR 461B-2049-TL, 49x17/26PR tire.

(4) Groove depth.- the mold skid depth or the groove depth after buffing.

TABLE A-1. (CONTINUED)

TEST CYCLE NR.	TEST VEL. (mph)	GROOVE DEPTH (Inches)	INFLATION PRESSURE (psi)	NORMAL LOAD (lbs)	TEST DEFL.
7P170	170	0.52	102 psi (F.P.),	$\approx$ 27500 lbs	= F.P. DEFL
7P180	180	(FULL)	ADJUST	@ 102 psi	@ 170 psi &
7P190	190		PRESS	F.P. &	39600 lbs
7P...*	...*		FOR F.W.	SPECIFIED	LOAD
7PV_{cr}	V_{cr}		CURVA-TURE	DEFL	
8P180	180	0.30			
8P...*	...*				
8PV_{cr}	V_{cr}				
9P200	200	0.10			
9P...*	...*				
9PV_{cr}	V_{cr}				
7L170	170	0.52	102 psi	@ $\approx$ 27500 lbs	
7L180	180	(FULL)		F.P. LOAD,	
7L190	190			ADJUST LOAD,	
7L...*	...*			LOAD	
7LV_{cr}	V_{cr}			FOR F.W. CURVA-	
8L180	180	0.30		TURE	
8L190	190				
8L...*	...*				
8LV_{cr}	V_{cr}				
9L200	200	0.10			
9L...*	...*				
9LV_{cr}	V_{cr}				

NOTES:

* Continue to increase the test speed in increments of 5 or 10 mph in subsequent test cycles until the critical speed (V_{cr}) is reached.

(1) F.P. - flat plate, F.W. - flywheel

(2) The second character in the test cycle number identifies the method taken to compensate for flywheel curvature, either by pressure ("P") increase or by load ("L") reduction.

(3) All approximations ($\approx$) were obtained from load-deflection curves, Goodyear report QTR 461B-2049-TL, 49x17/26PR tire.

(4) Groove depth.- the mold skid depth or the groove depth after buffing.

TABLE A-1. (CONTINUED)

TEST CYCLE NR.	TEST VEL. (mph)	GROOVE DEPTH (inches)	INFLATION PRESSURE (psi)	NORMAL LOAD (lbs)	TEST DEFL.
10P230	230	0.52	204 psi (F.P.)	$\approx$ 46000 lbs	= F.P. DEFL
10P240	240	(FULL)	ADJUST	@ 204 psi	@ 170 psi &
10P...*	...*		PRESS	F.P. &	39600 lbs
10PV_{cr}	V_{cr}		CURVA-TURE	SPECIFIED DEFL	LOAD
11P250	250	0.30			
11P...*	...*				
11PV_{cr}	V_{cr}				
10L230	230	0.52	204 psi	@ $\approx$46000 lbs	
10L240	240	(FULL)		F.P. LOAD,	
10L...*	...*			ADJUST	
10LV_{cr}	V_{cr}			LOAD FOR F.W.	
11L250	250	0.30		CURVA-	
11L260	260			TURE	
11L...*	...*				
11LV_{cr}	V_{cr}				

NOTES:

* Continue to increase the test speed in increments of 5 or 10 mph in subsequent test cycles until the critical speed (V_{cr}) is reached.

(1) F.P. - flat plate, F.W. - flywheel

(2) The second character in the test cycle number identifies the method taken to compensate for flywheel curvature, either by pressure ("P") increase or by load ("L") reduction.

(3) All approximations ($\approx$) were obtained from load-deflection curves, Goodyear report QTR 461B-2049-TL, 49x17/26PR tire.

(4) Groove depth.- the mold skid depth or the groove depth after buffing.

TABLE A-1. (CONTINUED)

TEST CYCLE NR.	TEST VEL. (mph)	GROOVE DEPTH (Inches)	INFLATION PRESSURE (psl)	NORMAL LOAD (lbs)	TEST DEFL.
12P220	220	0.52	170 psl (F.P.)	$\approx$ 24500 (lbs)	20% DEFL,
12P230	230	(FULL)	ADJUST	@ 170 psl	($\approx$2.52
12P240	240		PRESS	psl F.P. &	INCHES)
12P...*	...*		FOR F.W.	20% DEFL	
12PV_{cr}	V_{cr}		CURVA-TURE		
13P220	220			$\approx$10500 lbs	10% DEFL,
13P230	230			@ 170 psl	($\approx$1.26
13P...*	...*			psl F.P. &	INCHES)
13PV_{cr}	V_{cr}			10% DEFL	
12L220	220		170 psl	@ $\approx$24500 lbs	20% DEFL,
12L230	230			F.P. LOAD,	($\approx$2.52
12L240	240			ADJUST	INCHES)
12L...*	...*			LOAD	
12V_{cr}	V_{cr}			FOR F.W. CURVATURE	
13L220	220			@ $\approx$10500 lbs	10% DEFL,
13L230	230			F.P. LOAD,	($\approx$1.26
13L240	240			ADJUST	INCHES)
13L...*	...*			LOAD	
13V_{cr}	V_{cr}			FOR F.W. CURVATURE	

NOTES:

* Continue to increase the test speed in increments of 5 or 10 mph in subsequent test cycles until the critical speed (V_{cr}) is reached.

(1) F.P. - flat plate, F.W. - flywheel

(2) The second character in the test cycle number identifies the method taken to compensate for flywheel curvature, either by pressure ("P") increase or by load ("L") reduction.

(3) All approximations ($\approx$) were obtained from load-deflection curves, Goodyear report QTR 461B-2049-TL, 49x17/26PR tire.

(4) Groove depth.- the mold skid depth or the groove depth after buffing.

TABLE A-1. (CONTINUED)

TEST CYCLE NR.	TEST VEL. (mph)	GROOVE DEPTH (Inches)	INFLATION PRESSURE (psi)	NORMAL LOAD (lbs)	TEST DEFL.
14P190	190	0.52	136 psi (F.P.),	39600	$\approx$ F.P. DEFL
14P200	200	(FULL)	ADJUST		@ 136 psi &
14P...*	...*		PRESS		39600 lbs
14PV_{cr}	V_{cr}		FOR F.W.		LOAD
			CURVA-		
15P210	210	0.30	TURE		
15P...*	...*				
15PV_{cr}	V_{cr}				
16P220	220	0.10			
16P...*	...*				
16PV_{cr}	V_{cr}				
14L180	180	0.52	136 psi	39600 lbs	
14L...*	...*	(FULL)		(F.P.),	
14LV_{cr}	V_{cr}			ADJUST	
				LOAD	
15L190	190	0.30		FOR F.W.	
15L...*	...*			CURVA-	
15LV_{cr}	V_{cr}			TURE	
16L200	200	0.10			
16L...*	...*				
16LV_{cr}	V_{cr}				

NOTES:

* Continue to increase the test speed in increments of 5 or 10 mph in subsequent test cycles until the critical speed (V_{cr}) is reached.

(1) F.P. - flat plate, F.W. - flywheel

(2) The second character in the test cycle number identifies the method taken to compensate for flywheel curvature, either by pressure ("P") increase or by load ("L") reduction.

(3) All approximations ($\approx$) were obtained from load-deflection curves, Goodyear report QTR 461B-2049-TL, 49x17/26PR tire.

(4) Groove depth.- the mold skid depth or the groove depth after buffing.

45

TABLE A-1. (CONTINUED)

TEST CYCLE NR	TEST VEL (mph)	GROOVE DEPTH (Inches)	INFLATION PRESSURE (psi)	NORMAL LOAD (lbs)	TEST DEFL.
17P190	190	0.52	136 psi (F.P.),	$\approx$ 33000 lbs	= F.P. DEFL
17P...*	...*	(FULL)	ADJUST	@ 136 psi	@ 170 psi &
17PV_{cr}	V_{cr}		PRESS FOR F.W.	F.P. & SPECIFIED	39600 lbs LOAD
18P210	210	0.30	CURVA-	DEFL.	
18P...*	...*		TURE		
18PV_{cr}	V_{cr}				
19P230	230	0.10			
19P...*	...*				
19PV_{cr}	V_{cr}				
17L180	180	0.52	136 psi	@ $\approx$ 39600 lbs	
17L...*	...*	(FULL)		F.P. LOAD,	
17LV_{cr}	V_{cr}			ADJUST LOAD	
18L190	190	0.30		FOR F.W.	
18L...*	...*			CURVA-	
18LV_{cr}	V_{cr}			TURE	
19L200	200	0.10			
19L...*	...*				
19LV_{cr}	V_{cr}				

NOTES:
* Continue to increase the test speed in increments of 5 or 10 mph in subsequent test cycles until the critical speed (V_{cr}) is reached.

(1) F.P. - flat plate, F.W. - flywheel

(2) The second character in the test cycle number identifies the method taken to compensate for flywheel curvature, either by pressure ("P") increase or by load ("L") reduction.

(3) All approximations ($\approx$) were obtained from load-deflection curves, Goodyear report QTR 461B-2049-TL, 49x17/26PR tire.

(4) Groove depth - the mold skid depth or the groove depth after buffing.

46

TABLE A-1. (CONTINUED)

TEST CYCLE NR.	TEST VEL. (mph)	GROOVE DEPTH (Inches)	INFLATION PRESSURE (psl)	NORMAL LOAD (lbs)	TEST DEFL.
20P190 20P...* 20PV_{cr}	190 ...* V_{cr}	0.52 (FULL)	136 psl (F.P.) ADJUST PRESS FOR F.W. CURVA-TURE	≈ 21000 lbs @ 136 psl F.P. & 20% DEFL	20% DEFL (≈ 2.52 INCHES)
21P210 21P...* 21PV_{cr}	210 ...* V_{cr}	0.30			
22P220 22P...* 22PV_{cr}	220 ...* V_{cr}	0.10			
23P200 23P...* 23PV_{cr}	200 ...* V_{cr}	0.52 (FULL)		≈9000 lbs @ 136 psl F.P. & 10% DEFL	10% DEFL (≈ 1.26 INCHES)
24P210 24P...* 24PV_{cr}	210 ...* V_{cr}	0.30			
25P220 25P...* 25PV_{cr}	220 ...* V_{cr}	0.10			

NOTES:

* Continue to increase the test speed in increments of 5 or 10 mph in subsequent test cycles until the critical speed (V_{cr}) is reached.

(1) F.P. - flat plate, F.W. - flywheel

(2) The second character in the test cycle number identifies the method taken to compensate for flywheel curvature, either by pressure ("P") increase or by load ("L") reduction.

(3) All approximations (≈) were obtained from load-deflection curves, Goodyear report QTR 461B-2049-TL, 49x17/26PR tire.

(4) Groove depth.- the mold skid depth or the groove depth after buffing.

47

TABLE A-1. (CONTINUED)

TEST CYCLE NR.	TEST VEL. (mph)	GROOVE DEPTH (Inches)	INFLATION PRESSURE (psi)	NORMAL LOAD (lbs)	TEST DEFL.
20L190 20L...* 20LV_{cr}	190 ...* V_{cr}	0.52 (FULL)	136 psi	≈ 21000 lbs F.P. LOAD, ADJUST LOAD	20% DEFL (≈ 2.52 INCHES)
21L200 21L...* 21LV_{cr}	200 ...* V_{cr}	0.30		FOR F.W. CURVA- TURE	
22L210 22L...* 22LV_{cr}	210 ...* V_{cr}	0.10			
23L190 23L...* 23LV_{cr}	190 ...* V_{cr}	0.52 (FULL)		≈ 9000 lbs F.P. LOAD, ADJUST LOAD	10% DEFL (≈ 1.26 INCHES)
24L200 24L...* 24LV_{cr}	200 ...* V_{cr}	0.30		FOR F.W. CURVA- TURE	
25L210 25L...* 25LV_{cr}	210 ...* V_{cr}	0.10			

NOTES:

* Continue to increase the test speed in increments of 5 or 10 mph in subsequent test cycles until the critical speed (V_{cr}) is reached.

(1) F.P. - flat plate, F.W. - flywheel

(2) The second character in the test cycle number identifies the method taken to compensate for flywheel curvature, either by pressure ("P") increase or by load ("L") reduction.

(3) All approximations (≈) were obtained from load-deflection curves, Goodyear report QTR 461B-2049-TL, 49x17/26PR tire.

(4) Groove depth.- the mold skid depth or the groove depth after buffing.

TABLE A-1. (CONTINUED)

TEST CYCLE NR.	TEST VEL. (mph)	GROOVE DEPTH (Inches)	INFLATION PRESSURE (psi)	NORMAL LOAD (lbs)	TEST DEFL.
26P170 26P...* 26PV$_{cr}$	170 ...* V$_{cr}$	0.52 (FULL)	102 psi (F.P.), ADJUST PRESS FOR F.W. CURVA- TURE	$\approx$ 17000 lbs @ 102 psi F.P. & 20% DEFL	20% DEFL ($\approx$ 2.52 INCHES)
27P180 27P...* 27PV$_{cr}$	180 ...* V$_{cr}$	0.30			
28P190 28P...* 28PV$_{cr}$	190 ...* V$_{cr}$	0.10			
29P180 29P...* 29PV$_{cr}$	180 ...* V$_{cr}$	0.52 (FULL)		$\approx$ 8000 lbs @ 136 psi F.P. & 10% DEFL	10% DEFL ($\approx$ 1.26 INCHES)
30P190 30P...* 30PV$_{cr}$	190 ...* V$_{cr}$	0.30			
31P200 31P...* 31PV$_{cr}$	200 ...* V$_{cr}$	0.10			

NOTES:

* Continue to increase the test speed in increments of 5 or 10 mph in subsequent test cycles until the critical speed (V$_{cr}$) is reached.

(1) F.P. - flat plate, F.W. - flywheel

(2) The second character in the test cycle number identifies the method taken to compensate for flywheel curvature, either by pressure ("P") increase or by load ("L") reduction.

(3) All approximations ($\approx$) were obtained from load-deflection curves, Goodyear report QTR 461B-2049-TL, 49x17/26PR tire.

(4) Groove depth.- the mold skid depth or the groove depth after buffing.

TABLE A-1. (CONTINUED)

TEST CYCLE NR.	TEST VEL. (mph)	GROOVE DEPTH (Inches)	INFLATION PRESSURE (psi)	NORMAL LOAD (lbs)	TEST DEFL.
26L160 26L...* 26LV_{cr}	160 ...* V_{cr}	0.52 (FULL)	102 psi	≈ 17000 lbs F.P. LOAD, ADJUST LOAD FOR F.W. CURVA- TURE	20% DEFL (≈ 2.52 INCHES)
27L170 27L...* 27LV_{cr}	170 ...* V_{cr}	0.30			
28L180 28L...* 28LV_{cr}	180 ...* V_{cr}	0.10			
29L160 29L...* 29LV_{cr}	160 ...* V_{cr}	0.52 (FULL)		≈ 8000 lbs F.P. LOAD, ADJUST LOAD FOR F.W. CURVA- TURE	10% DEFL (≈ 1.26 INCHES)
30L170 30L...* 30LV_{cr}	170 ...* V_{cr}	0.30			
31L180 31L...* 31LV_{cr}	180 ...* V_{cr}	0.10			

NOTES:
* Continue to increase the test speed in increments of 5 or 10 mph in subsequent test cycles until the critical speed (V_{cr}) is reached.
(1) F.P. - flat plate, F.W. - flywheel
(2) The second character in the test cycle number identifies the method taken to compensate for flywheel curvature, either by pressure ("P") increase or by load ("L") reduction.
(3) All approximations (≈) were obtained from load-deflection curves, Goodyear report QTR 461B-2049-TL, 49x17/26PR tire.
(4) Groove depth.- the mold skid depth or the groove depth after buffing.

ABBREVIATIONS, ACRONYMS, and SYMBOLS

a Distance taken normal to the tire plane centerline from centerline to point of application of force Q

A_R Tire aspect ratio

C_z Empirical load/deflection constant

d Tire vertical deflection

d_r Tire rated vertical deflection

D_o Tire outside diameter

dh Radial growth due to centrifugal effects

dm Differential mass element per unit width of tread

E Modulus of elasticity

E_f Fabric modulus of elasticity

E_r Rubber-tread modulus of elasticity

EI Bending stiffness of tread band treated as a beam

F_c Carcass force

F_z Vertical load

g Gravity constant

h Tire section height

k Foundation spring rate of the tread band

K_z Tire vertical stiffness, slope of the vertical load/deflection curve

l Cord length

L Length of beam

m_t Total tire mass

p_i Tire inflation pressure

p_r Tire rated inflation pressure

Q Centrifugal force equivalent to half the total centrifugal force acting on the tire cross-section

r_o Tire rolling radius

t time or average thickness of tread and carcass at the tire crown

T Tension force in tread band

t_f Thickness of the cord-rubber fabric region

t_r Thickness of the rubber-tread region

U Internal potential energy

U_{ef} Internal energy due to the elastic foundation

U_{se} Strain energy

v wave speed

V External potential energy

V_{cr} Critical speed

V_d External potential energy due to distributed loads

V_t External potential energy due to tension

w Vertical beam deflection

W_t Total tire weight

w_s Cross-sectional width

x Longitudinal distance along the beam axis

51

z Radial tire distance from cross-section centroid

δ First-order variation

δW_e Virtual work performed by external forces

δW_i Virtual work performed by internal forces

σ_{xx} Longitudinal stress

γ Cord half angle

ρ Tread density

ρ_1 Mass per unit area of tire surface

ρ' Effective tread density

ρ_m Average tread mass density

ϵ_{xx} Longitudinal strain

ω Tire rotational speed

END

DATE
FILMED
8-88
DTIC